Large deformation, damage evolution and failure of ductile structures to pulse-pressure loading

Y. Yuan, P. J. Tan*, K. A. Shojaei, P. Wrobel

Department of Mechanical Engineering, University College London, Torrington Place, London WC1E 7JE, UK

Abstract

In this paper, a model is developed for an elastic perfectly-plastic structural beam system subjected to general pulse-pressure loadings - this may be either impulsive or non-impulsive - which is capable of capturing large non-linear deformation, ductile damage evolution and its consequential failure. The proposed model is an extension of Schleyer and Hsu (2000) by incorporating interactions between bending, membrane stretch and transverse shear in the fully plastic stress state, and uses damage mechanics to capture the loss of integrity at the supports and the subsequent beam detachment. Predictions by the model were validated against existing experimental data from literature and to three-dimensional finite element models developed in this paper. Parametric studies were performed to elucidate the effects of loading duration on the mode of deformation by the beam and the critical conditions governing their transition. The efficacy of Youngdahl's technique (Youngdahl, 1970, 1971) on desensitising pulse shape effects is also investigated using different pressure pulse profiles and it will be shown that the technique is successful only for monotonically decaying pulse-pressures.

*Corresponding author Tel: +44 (0)20 7679 3754
Email address: pj.tan@ucl.ac.uk (P. J. Tan)

June 15, 2016

Keywords: Non-impulsive loadings, large deformation, damage modes, pulse shape, Youngdahl's approximation

1. Introduction

The deformation and damage of ductile structural components - beams, plates and shells - to intense pulse-pressure loading are especially pertinent to the nuclear, offshore and defence industries. Of particular interests is their response to pulse-pressure loading, such as one generated by a blast. A considerable body of literature exists that dealt with the response of structures to short-duration, high-intensity transverse pressure pulses (referred to, hereinafter, as impulsive loadings) where the duration of the pulse is insignificant compared to the natural response time of the structure. In real-life, however, the majority of these pulses are, in fact, non-impulsive - this is typically the case if the source of an explosion occurs at a considerable standoff distance from the target structure (Ramajeyathilagam and Vendhan, 2004; Langdon et al., 2014; Spranghers et al., 2013). The comparatively limited literature on how structures respond to intense non-impulsive loadings is one of the motivations behind the present work.

Menkes and Opat (1973) identified three distinct damage modes that are characteristics of clamped ductile beams subjected to impulsive loadings: viz. mode I - large inelastic deformation; mode II - tensile tearing over the support; mode III - transverse shear failure at the support. The terms 'deformation modes' and 'damage modes' are often used interchangeably. Of note is that damage in modes II and III always initiates in the region of the beam abutting the support although, in reality, a sharp distinction between the two modes is not found. There exist several analytical models - Jones (1976), Yu and Chen (2000), Shen and Jones (1992), Wen (1996) and Alves and Jones (2002a,b) to name a few - on predicting the critical impulses cor-

responding to mode transitions. However, nearly all were formulated within the constitutive framework of limit analysis and assumed impulsive loading conditions. The model by Jones (1976) proposed that the critical impulsive velocity for mode I→II occurs when the maximum in-plane strain - arising from catenary (membrane) and bending actions - over the supports reaches the critical tensile strain of the material from which the beam is made; and when the maximum transverse shear sliding at the support reaches the beam thickness for the corresponding mode III damage. In reality, however, membrane forces must play a significant role during failure in mode III and, likewise, with transverse shear force in mode II. To address this, Shen and Jones (1992) developed an energy-based failure criterion to account for the simultaneous influence of bending, membrane stretch and transverse shear that is applicable to a broad class of dynamic structural problems. It states that damage (either in mode II or III) occurs when the specific dissipation (density of plastic work) θ at a point in the structure reaches a critical value of $\theta_c = \int_0^{\epsilon_r} \sigma_d \mathrm{d}\epsilon$ where ϵ_r and σ_d are the true rupture strain and the true dynamic stress of a uniaxial tensile test, respectively, which they assumed are equal to the equivalent strain and stress in the actual structure. They found that transition from mode II to III occurs at the critical value of $\beta_c = 0.45$, where β is the ratio of the plastic work absorbed through shearing deformation to the total plastic work done by all the stress components. Yu and Chen (2000) studied transverse plastic shear failure at the support in mode III where the efficacy of $\beta_c = 0.45$, previously obtained by Shen and Jones (1992), was assessed against different forms of interactive yield criteria; furthermore, the weakening effects of the sliding sections - treated as a transverse-displacement discontinuity - during the failing process is also included in their model.

Although predictions for critical impulses by the aforementioned agree reasonably well with experimental data by Menkes and Opat (1973), all the models were formulated within the constitutive framework of limit analysis

which disregards the influence of material elasticity. Whether these rigid-plastic methods of analysis provide an acceptable approximation of the dynamic response of actual elasto-plastic structures is, consequently, an important issue. Symonds (1985) showed that a rigid-plastic analysis may be acceptable if the energy ratio $R \gg 1$, where R is the ratio of the total energy imparted by the loading E_{in} to the maximum elastic strain energy capacity $U_e^{\max}$ of the structure given by

$$R = \frac{E_{\text{in}}}{U_e^{\max}}. \tag{1}$$

This problem was re-investigated by Symonds and Frye (1988) through a single-degree-of-freedom (SDOF) mass spring model - using either an elastic perfectly-plastic or rigid perfectly-plastic spring - where it was found that a large energy ratio ($R \gg 1$) is a necessary, but not a sufficient, condition for a rigid-plastic approximation. If the duration of the load pulse is not brief in comparison to the fundamental period of elastic vibration of the structure, a rigid-plastic idealisation would lead to an unacceptably high error, by as much as 60%. In some cases this error may even be negative, i.e. the rigid-plastic solution grossly underestimates the final deformation of the structure (Stronge and Yu, 1993). Subsequent investigation by Yu (1993) on how elasticity affects the dynamic plastic response of cantilever beams showed that both the pulse shape and its rise time have a significant influence on the final beam deformation.

It is evident that existing models based on rigid-plastic methods cannot be used to study the dynamic response of elasto-plastic beams subjected to intense non-impulsive loadings. In addition, it is unclear as to how pulse shape, and its duration, influence the mode of deformation and how limits to deformation due to necking localisation and/or ductile fracture affects the final performance of a structure. The aforementioned issues are addressed in this paper which will present the results of a detailed analytical and numer-

ical study. To this end, a model is developed for an elastic perfectly-plastic structural beam system which is sufficiently general to (1) model large elasto-plastic deformation with catenary actions; (2) incorporate the interactions between bending, membrane and shear in the yield and plastic limit functions; (3) model the loss of integrity at the supports through ductile damage evolution and its subsequent catastrophic failure; and, (4) account for general (impulsive and non-impulsive) loading conditions. For the sake of definiteness, *damage* shall refer to the onset and subsequent degradation of the generalised stresses in the beam, and at its supports, as opposed to *failure* which will refer to a complete loss of load carrying capacity, exemplified by the catastrophic detachment of the beam from its supports.

The outline of this paper is as follows: Section 2 presents the development of the structural beam system model; details of the finite element model is given in Section 3; in Section 4, a comparison between the analytical, numerical predictions, and the experimental results is made; and, Section 5 presents the results of the parametric studies to elucidate the effects of pulse duration and pulse shape on the deformation and mode of damage in elasto-plastic beams.

2. Formulation of an elasto-plastic structural beam system

The model by Schleyer and Hsu (2000) will be extended here to include the following additional features: (1) The effects of transverse shear force at the support were previously neglected which were known to play a key role in modes II and III (Li and Jones, 2000; Shen and Jones, 1992). The current model accounts for this through the introduction of a vertical spring at the support; (2) A 'square' fully plastic stress condition was used previously to decouple the interactions between bending moment and membrane force following plastic hinge formation. The current model incorporates an interactive fully plastic stress condition to allow the simultaneous influence

of transverse shear, axial membrane force and bending moment to be considered; (3) It was previously assumed that a static plastic hinge forms either at the support or/and the mid-span of the beam when the corresponding fully plastic stress condition is met. The current model incorporates travelling plastic hinges; and (4) Predictions by Schleyer and Hsu (2000) were confined to the mid-span deflection in mode I since it did not consider the weakening effects of damage and failure. The current model introduces progressive damage to capture the loss of integrity at the supports and its subsequent detachment to capture damage in modes II and III.

2.1. Features of the structural beam system

Figure 1 shows a schematic of a structural beam system which consists of a ductile beam member supported at each end by three springs (one rotational and two axials). The beam - made of a rate-independent, elastic perfectly-plastic material in the present study - is of total length $2L$ and a uniform rectangular cross-section of thickness H and width B where $L/H \gg 1$ (i.e. the beam is slender). Following Shen and Jones (1992), a pulse-pressure loading $p(t)$ is assumed to always impinge normally, and uniformly, over its entire span regardless of its subsequent transverse deflection. The pressure pulse can be of any general form: exponentially decaying (EXP), linearly decaying (LIN), rectangular (REC) etc.

The rotational springs possess elasto-plastic characteristics to model the beam rotation at each end and the subsequent plastic hinge formation. Both the axial and vertical springs have rigid-plastic characteristics to model the 'plastic stretch' and 'plastic shear sliding' actions at the support, respectively. Collectively, the trio of springs may be regarded as a representation of a fully-clamped boundary which allows interactions between bending, stretch and shear to be considered and where damage mechanics will be applied to model the progressive loss of support integrity. It is worth noting that both experi-

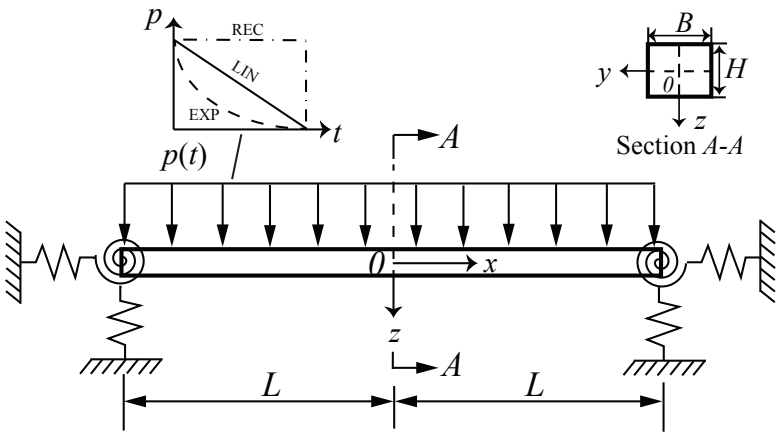

Figure 1: Schematic of the structural beam system. A plane of geometric and loading symmetry exists along $x = 0$, $-B/2 \leq y \leq B/2$, $-H/2 \leq z \leq H/2$ so that only the right-half needs to be modelled.

ments and analytical studies (Menkes and Opat, 1973; Shen and Jones, 1992; Wen, 1996) have previously shown that damage (mode II and III) occurs in the region abutting the support for impulsively-loaded beams. In the case of non-impulsive loads, the present model, too, assumes that failure occurs in the same region of the beam member. Detailed three-dimensional (3D) finite-element simulations, to be presented later in Section 4, will show that this is, indeed, the case. A plane of geometric and loading symmetry exists at the mid-span of the beam ($x = 0$), thus permitting one-half of the beam to be analysed.

2.2. Fully plastic stress state

The components of stress σ on any cross-section of the beam member, including at its supports, give the following stress resultants for axial force N, shear force Q, axial torque T and bending moment M (Stronge and Yu,

1993):

$$N = \int_A \sigma_{xx} \mathrm{d}A, \quad Q = \int_A \sigma_{xz} \mathrm{d}A, \quad T = \int_A (y\sigma_{xz} - z\sigma_{xy}) \mathrm{d}A, \quad M = -\int_A z\sigma_{xx} \mathrm{d}A \tag{2}$$

where A is the cross-sectional area of the beam; y and z are transverse coordinates measured from the axis through the centroid of every section. Since the beam is loaded by equal but opposing couples that act in directions perpendicular to the plane of symmetry, the beam must bend in the plane of symmetry and does not twist, i.e. $T = 0$. For slender beam members where $L/H \gg 1$, stress resultants arising from the actions of membrane N, shear Q and bending M are analogous to stress components in a continuum and are referred, hereinafter, as generalised stresses (Stronge and Yu, 1993; Jones, 1989; Shen and Jones, 1992).

The fully plastic limit function ψ^p for generalised stresses in a rectangular cross-section is given by (Stronge and Yu, 1993)

$$\psi^p = \frac{|M|}{M_0}\sqrt{1 - \frac{Q^2}{Q_0^2}} + \frac{N^2}{N_0^2} + \frac{Q}{Q_0} - 1 \tag{3}$$

where $M_0 = \sigma_Y BH^2/4$, $N_0 = \sigma_Y BH$ and $Q_0 = 2\sigma_Y BH/3\sqrt{3}$ are the fully plastic bending moment, in-plane membrane force and transverse shear force, respectively; σ_Y is the static yield strength. It is convenient to express Eq. 3 in non-dimensional form as follows:

$$\psi^p = |\bar{M}|\sqrt{1 - \bar{Q}^2} + \bar{N}^2 + \bar{Q}^2 - 1 \tag{4}$$

where $\bar{M} = M/M_0$, $\bar{N} = N/N_0$ and $\bar{Q} = Q/Q_0$ are the non-dimensional fully plastic generalised stresses. The fully plastic stress condition $\psi^p = 0$ is an upper bound for stress states that satisfy yield in any part of the cross-section. This bound for the fully plastic state is based on a simplifying assumption that the distribution of normal stress in the fully plastic stress state with,

or without, shear is identical (Stronge and Yu, 1993). Plastic hinge forms at any cross section where $\psi^p = 0$ is reached.

2.3. Damage initiation and evolution

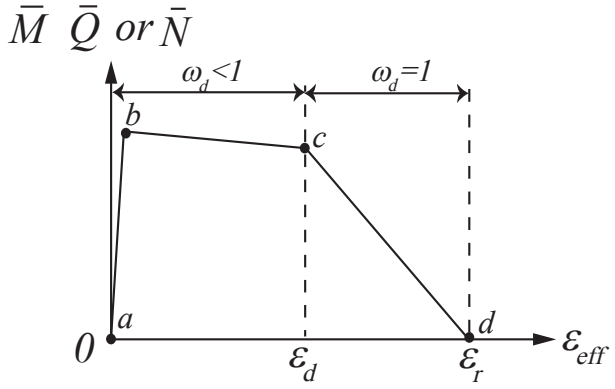

Figure 2: Schematic showing non-dimensional generalised stresses as a function of effective strain pre - ($\omega_d < 1$) and post - ($\omega_d = 1$) damage initiation.

In this study, *damage* - not to be confused with 'damage modes' used by Menkes and Opat (1973) - shall refer to the onset and subsequent degradation of the generalised stresses in the beam member and at its supports. Figure 2 shows a schematic of the generalised stresses ($\bar{M}$ or $\bar{N}$ or $\bar{Q}$) versus effective strain ϵ_{eff} where points b and c, respectively, indicate the generalised stress state on any cross-section where the fully plastic stress condition ($\psi^p = 0$) and the damage initiation criterion ($\omega_d = 1$) are first satisfied. Thus, the states of stress along segment $b - c$ correspond to any cross-section that is fully plastic but does not yet meet the damage initiation criterion, given later in Eq. 12. Upon damage initiation, the generalised stresses degrade in accordance to an evolution law, denoted by the line $c - d$. This section presents the damage initiation criterion and an evolution law that governs the softening of these generalised stresses.

In general, the effective strain ϵ_{eff} on any cross-section may be expressed as

(Wen, 1996; Alves and Jones, 2002a)

$$\epsilon_{\text{eff}} = \sqrt{\frac{2}{9}\Big[(\epsilon_{xx}-\epsilon_{yy})^2 + (\epsilon_{yy}-\epsilon_{zz})^2 + (\epsilon_{xx}-\epsilon_{zz})^2 + \frac{3}{2}(\gamma_{xz}^2+\gamma_{zy}^2+\gamma_{xy}^2)\Big]}. \tag{5}$$

For slender beams, it is reasonable to assume that $\epsilon_{yy} = \epsilon_{zz} = -\epsilon_{xx}/2$ and $\gamma_{xy} = \gamma_{yz} = 0$ (Wen, 1996; Alves and Jones, 2002a). Hence, Eq. 5 reduces to

$$\epsilon_{\text{eff}} = \sqrt{\epsilon_{xx}^2 + \frac{1}{3}\gamma_{xz}^2}. \tag{6}$$

The total in-plane strain ϵ_{xx} through any cross-section x comprises of two parts given by (Wen, 1996; Jones, 1976)

$$\epsilon_{xx} = \epsilon_m + \epsilon_b \tag{7}$$

where the membrane strain ϵ_m and bending strain ϵ_b may be expressed, respectively, as functions of the transverse mid-span displacement of the beam W_B given by

$$\epsilon_m = 2\left(\frac{W_B}{L}\right)^2\left(\frac{x}{L}\right)^2 \tag{8}$$

and

$$\epsilon_b = \frac{W_B H}{L^2}\left(\frac{x}{L}\right). \tag{9}$$

Following Wen (1996), Alves and Jones (2002a), Yu and Chen (2000) and Jones (1976), it is further assumed that the transverse shear strain γ_{xz} is negligible in the beam member but is dependent upon the plastic shear sliding distance over the shear band at the support. Hence, on any cross-section

$$\gamma_{xz} = \begin{cases} 0 & \text{if } 0 \le x < L \\ W_S/(l/2) & \text{if } x = L \end{cases} \tag{10}$$

where W_S is the plastic shear sliding displacement. Note that l is the width of the shear band and, following Jones (1976), it is assumed that $l = 2H$.

Substituting Eqs. 7 - 10 into Eq. 6, gives an approximate expression for the effective strain on any cross-section x as follows:

$$\epsilon_{\text{eff}} = \begin{cases} \dfrac{2\left(\frac{W_B}{L}\right)^2\left(\frac{x}{L}\right)^2 + \left(\frac{W_B}{L}\right)\left(\frac{x}{L}\right)\left(\frac{H}{L}\right)}{\sqrt{\left[2\left(\frac{W_B}{L}\right)^2 + \left(\frac{W_B}{L}\right)\left(\frac{H}{L}\right)\right]^2 + \frac{1}{3}\left(\frac{W_S}{H}\right)^2}} & \text{if } 0 \leq x < L \\ & \text{if } x = L \end{cases} \tag{11}$$

It is noted that the effective strain is greatest at the support where $x = L$ since its two constituent components (total axial in-plane and transverse shear strains) are both highest there. This is in agreement with Wen (1996) and Alves and Jones (2002a). Expressions for W_B and W_S are to be derived in Section 2.5.

The criterion for damage initiation is met when (ABAQUS, 2010)

$$\omega_d = \frac{\epsilon_{\text{eff}}}{\epsilon_d} = 1 \tag{12}$$

where ω_d is a state variable that increases monotonically with effective strain ϵ_{eff} and ϵ_d is the effective strain at the onset of damage. Upon the initiation of damage, i.e. $\omega_d = 1$, progressive softening of the non-dimensional generalised stresses follows

$$|\bar{M}| = |\bar{M}^f|(1-D), \quad \bar{N} = \bar{N}^f(1-D) \quad \text{and} \quad \bar{Q} = \bar{Q}^f(1-D) \tag{13}$$

where D is the damage variable; $\bar{M}^f$, $\bar{N}^f$ and $\bar{Q}^f$ are the non-dimensional bending moment, membrane force and transverse shear force at the onset of damage, respectively. For the sake of simplicity, a linear evolution of the damage variable D with effective strain ϵ_{eff} is adopted here as follows: (ABAQUS, 2010)

$$D = \frac{\epsilon_{\text{eff}} - \epsilon_d}{\epsilon_r - \epsilon_d} \tag{14}$$

where ϵ_r is the rupture strain in a uniaxial tensile test. This definition ensures

that when $D = 1$, generalised stresses reduces to zero.

2.4. Failure criteria

Failure shall refer to a complete loss of load carrying capacity by the beam member through complete detachment from its supports. Experiments by Menkes and Opat (1973) have shown that an impulsively loaded beam always fails at its supports for modes II and III; this is also in agreement with predictions by the analytical models of Wen (1996) and Alves and Jones (2002a). Here, Eq. 11 too shows that ϵ_{eff} is greatest at the support ($x = L$) where damage is expected to initiate and evolve. Therefore, failure criteria need only be established for the supports in Fig 1.

The criteria delineating the different modes of failure, identified by Menkes and Opat (1973), are as follows:

$$\text{Mode I}: \quad D < 1, \quad \omega_s < 1 \tag{15a}$$

$$\text{Mode II}: \quad D = 1, \quad \omega_s < 1 \tag{15b}$$

$$\text{Mode III}: \quad D = 1, \quad \omega_s \geq 1 \tag{15c}$$

The state variable ω_s is expressed as

$$\omega_s = \frac{\beta}{\beta_c} = 1, \tag{16}$$

where β is the ratio of the plastic work absorbed through shearing deformation to the total plastic work done by all the stress components given by (Shen and Jones, 1992)

$$\beta = \frac{E_S^s}{E_S^s + E_S^b + E_S^m} \tag{17}$$

where E_S^s is the shear strain energy obtained via the vertical spring; E_S^b is the

bending strain energy of the rotational spring; E_S^m is the membrane strain energy obtained via the horizontal axial spring; and, β_c is the critical β value marking the transition from mode II to III. For aluminium beams, Yu and Chen (2000) have found that β_c corresponding to a square yield criterion is larger than 0.45 by Shen and Jones (1992) for an interactive yield criterion. Furthermore, they also found that β_c is a material-dependent parameter which is independent of geometry. Since an interactive fully plastic limit function is used here and material properties corresponding to Aluminium 6061-T6 - the same as Shen and Jones (1992) and Yu and Chen (2000) - is used in the FE simulations to be presented in Section 4, it is reasonable to assume that $\beta_c = 0.45$.

2.5. Equations of motion

The transverse displacement at any point x ($x > 0$) of the structural beam system may be approximated as a sum of n generalised displacements and mode functions given by (Williams, 1996)

$$W(x,t) = \sum_{i=1}^{n} \phi_i(x) w_i(t) \tag{18}$$

where the partial functions $\phi_i(x)$ are admissible mode functions that satisfy the geometric boundary conditions and the temporal functions $w_i(t)$ are generalised transverse displacements to be determined by the Lagrange equations of the 2nd kind. Since the transverse displacement is represented here by the sum of polynomials, instead of the normal modes of transverse vibration in a beam system, $\phi_i(x)$ need not be orthogonal (Williams, 1996). According to Eq. 18, the displacement at the mid-span and support are given, respectively, by

$$W_B(t) = W(x = 0, t) \quad \text{and} \quad W_S(t) = W(x = L, t). \tag{19}$$

The corresponding velocity ($\dot{W}$) and acceleration ($\ddot{W}$) fields also use the same partial functions given by

$$\dot{W}(x,t) = \sum_{i=1}^{n} \phi_i(x)\dot{w}_i(t) \quad \text{and} \quad \ddot{W}(x,t) = \sum_{i=1}^{n} \phi_i(x)\ddot{w}_i(t). \tag{20}$$

Defining the generalised mass of the beam as

$$M_{ij} = \begin{cases} m\int_0^L \phi_i(x)\phi_j(x)\mathrm{d}x & \text{if } i \neq j \\ m\int_0^L \phi_i^2(x)\mathrm{d}x & \text{if } i = j \end{cases} \tag{21}$$

where m is the mass per unit length, the total kinetic energy of the beam system at any given time t can be expressed as

$$E^K = \frac{1}{2}m\int_0^L \dot{W}^2(x,t)\mathrm{d}x = \frac{1}{2}\sum_{i}^{n}\sum_{j}^{n} M_{ij}\dot{w}_i\dot{w}_j. \tag{22}$$

The total potential (strain) energy of the entire beam system is

$$E^P = \underbrace{E_S^b + E_S^s + E_S^m}_{\text{support}} + \underbrace{E_B^b + E_B^m}_{\text{beam}} \tag{23}$$

where E_B^b and E_B^m are the bending and membrane strain energies of the beam member, respectively; E_S^s, E_S^b and E_S^m are the shear, bending and membrane strain energies associated with the vertical, rotational and axial springs, respectively, at the supports. Note that subscripts S and B are used here to denote support and beam member, respectively; whilst, superscripts s, b and m denote shear, bending and membrane, respectively. The generalised force is given by

$$Q_i = p(t)\int_0^L \phi_i(x)\mathrm{d}x, \quad i = 1, 2, ..., n. \tag{24}$$

Since the *Lagrangian* of the structural beam system is

$$\mathcal{L} = E^K + V, \tag{25}$$

the differential equations governing w_i are obtained by substituting Eqs. 25 and 24 into the well-known Lagrange equation of the 2nd kind

$$\frac{\mathrm{d}}{\mathrm{d}t}\left(\frac{\partial \mathcal{L}}{\partial \dot{w}_i}\right) + \frac{\partial \mathcal{L}}{\partial w_i} = Q_i, \quad i = 1, 2, ..., n \tag{26}$$

to give

$$\sum_{j=1}^{n} M_{ij}\ddot{w}_j + \frac{\partial E^P}{\partial w_i} = p(t)\int_0^L \phi_i(x)\mathrm{d}x, \quad i = 1, 2, ..., n. \tag{27}$$

The key to obtaining the governing equations of motion in Eq. 27 is to derive the various strain energy components (E_S^b, E_S^s, E_S^m, E_B^b and E_B^m) in Eq. 23. Following Schleyer and Hsu (2000) and Biggs (1964), the dynamic response of the beam system will be divided into three separate phases and the strain energy components corresponding to each are derived in the following subsections.

Note that each phase of motion has its own unique set of initial conditions and associated displacement (and velocity) field. In the present study, the transitional conditions between phases follow the proposal by Symonds et al. (1984), which is based on the well-known 'minimum Δ_0 technique'. This technique is commonly employed to determine the starting amplitude of the 'new' velocity field by minimising the difference in kinetic energies between the velocity fields at the end of the terminating phase and at the start of the new phase (Schleyer and Hsu, 2000; Langdon and Schleyer, 2005; Stronge and Yu, 1993).

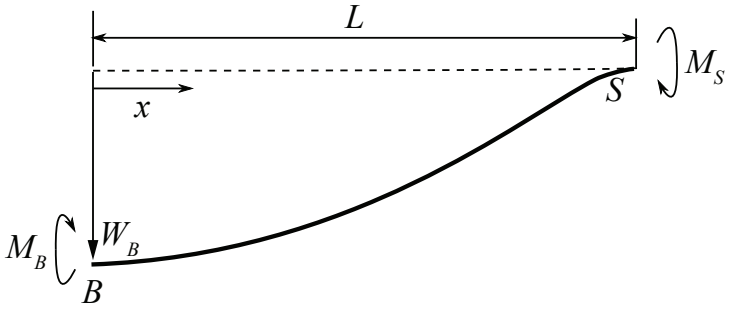

Figure 3: Schematic of the transverse displacement for the right-half of the structural beam system in Phase I.

2.5.1. Phase I: $0 < t \leq t_1$

In Phase I, it is reasonable to neglect catenary actions and transverse shear since the transverse deflection is small compared to the beam thickness, i.e. $W_B \ll H$ (Izzuddin, 2005; Schleyer and Hsu, 2000). To simplify the transition from an elasto-plastic to a fully plastic stress state, the true moment-curvature relationship on any cross-section - with its non-linear increase in yield moment M_Y to the fully plastic bending moment M_0 (shown schematically in Fig 4) - is replaced by a bilinear approximation to simplify the calculations of the bending moment (Jones, 1989; Schleyer and Hsu, 2000; Izzuddin, 2005). Since bending moment is always greatest at either the support ($x = L$) or the mid-span ($x = 0$) of the transversely-loaded beam, one should expect a plastic hinge to form first at either of these two locations (Biggs, 1964; Schleyer and Hsu, 2000; Izzuddin, 2005; Langdon and Schleyer, 2005). Consequently, fully plastic limit function given by Eq. 4 need only be defined at the support and mid-span of the beam, respectively, as follows:

$$\psi_S^p = |\bar{M}_S| - 1 \tag{28}$$

and

$$\psi_B^p = |\bar{M}_B| - 1. \tag{29}$$

Phase I motion ends when either $\psi_S^p = 0$ or $\psi_B^p = 0$: whichever is reached first. Notwithstanding, Schleyer and Hsu (2000) and Fallah et al. (2013)

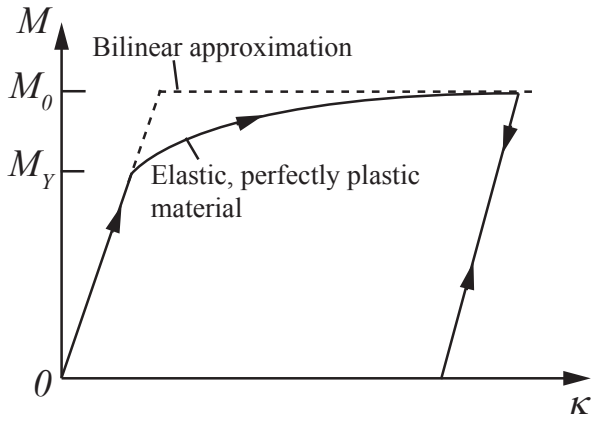

Figure 4: Bilinear approximation of the moment-curvature characteristics for an elastic-perfectly plastic beam system with a rectangular cross-section.

have shown that the sequence of hinge formation depends critically on the non-dimensional parameter $\alpha(= K_\phi L/EI)$, where E is Young's modulus and $I = BH^3/12$ is the beam's second moment of area. Fallah et al. (2013) found that when $\alpha > 6$, a plastic hinge always forms at the support first. To ensure that the horizontal and vertical axial springs are always perpendicular, a relatively large rotational stiffness $K_\phi = 10^8$ N/m is used as suggested by Schleyer and Hsu (2000). Therefore, it is reasonable to assume that a plastic hinge always forms first at the support since $\alpha \gg 6$.

Following Schleyer and Hsu (2000), an admissible transverse displacement field for the right-half of the structural beam system in Phase I is

$$W(x,t) = \frac{w_1(t)}{2}\left(1 + \cos\frac{\pi x}{L}\right) + w_2(t)\cos\frac{\pi x}{2L}. \tag{30}$$

The bending strain energies in the beam member and rotational spring are,

respectively,

$$E_B^b(t) = \frac{EI}{2}\int_0^L \left[\frac{\partial^2 W(x,t)}{\partial x^2}\right]^2 \mathrm{d}x \tag{31}$$

and

$$E_S^b(t) = \frac{K_\phi}{2}\phi(t)^2 \tag{32}$$

where $\phi(t) = \int_0^L [\partial^2 W(x,t)/\partial x^2]\mathrm{d}x$ (Langdon and Schleyer, 2005; Schleyer and Hsu, 2000). Since $W_B \ll H$, it is reasonable to assume that the strain energies due to shear and membrane are negligibly small (Izzuddin, 2005); hence,

$$E_S^s(t) = E_S^m(t) = E_B^m(t) \simeq 0. \tag{33}$$

Substituting Eqs. 31, 32 and 33 into Eq. 27, and using the initial conditions $w_1 = w_2 = 0$ and $\dot{w}_1 = \dot{w}_2 = 0$ gives the two equations of motion for this phase. When the fully plastic stress condition at the support is reached, i.e.

$$\psi_S^p = |K_\phi \phi(t)|/M_0 - 1 = 0, \tag{34}$$

it marks the end of Phase I deformation at the corresponding time of $t = t_1$.

2.5.2. Phase II: $t_1 < t \leq t_2$

In Phase II, the beam member may be assumed to deform in a manner similar to a simply supported beam - see Biggs (1964). Following Izzuddin (2005), Fallah and Louca (2007) and Fallah et al. (2013), small transverse deflection is also assumed for Phase II; hence, the influence of transverse shear and catenary actions are also ignored. Therefore, the fully plastic stress condition at the support - since $\psi_S^p = 0$ - reduces to

$$|\bar{M}_S| = 1 \tag{35}$$

whilst the same at the mid-span simplifies to

$$\psi_B^p = |\bar{M}_B| - 1. \tag{36}$$

Phase II motion ends when $\psi_B^p = 0$.

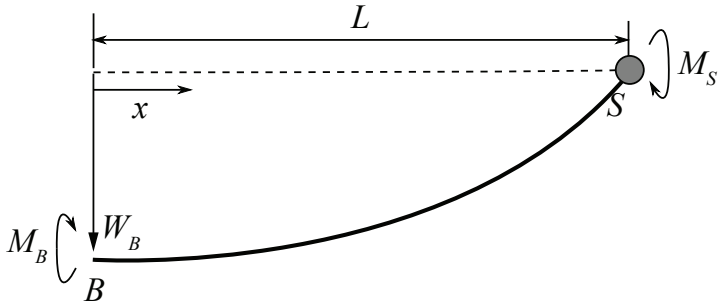

Figure 5: Schematic of transverse displacement profile for the right-hand half of the structural beam system in Phase II.

An admissible transverse displacement field for Phase II motion is (Schleyer and Hsu, 2000)

$$W(x,t) = \Big[w_1(t_1) + w_2(t)\Big] \cos\frac{\pi x}{2L} \tag{37}$$

where $w_1(t_1)$ is the terminating amplitude of the generalised displacement from Phase I at t_1. Expressions for strain energy components are identical to those previously derived for Phase I (Eq. 31 for E_B^b; Eq. 33 for E_B^m, E_S^s and E_S^m) with the notable exception of the bending strain energy of the rotational spring at the support which is as follows:

$$E_S^b(t) = |M_S|[\phi(t) - \phi_1] = M_0[\phi(t) - \phi_1] \tag{38}$$

where $\phi_1 = M_0/K_\phi$. Substituting Eqs. 31, 33 and 38 into Eq. 27 gives the equation of motion for Phase II. Following Symonds et al. (1984), the starting amplitude of the generalised velocity in this phase is given by

$$\dot{w}_2 = \frac{8}{3\pi}\dot{w}_1(t_1) + \dot{w}_2(t_1) \tag{39}$$

where $\dot{w}_1(t_1)$ and $\dot{w}_2(t_1)$ refer to the terminating amplitude of the generalised velocity from Phase I at time t_1. Once the mid-span of the beam meets the fully plastic stress condition, i.e.

$$\psi_B^p = EI\kappa(t)/M_0 - 1 = 0 \tag{40}$$

where $\kappa(t) = \partial^2 W(x,t)/\partial x^2|_{x=0}$ is the curvature at the mid-span, it marks the end of Phase II deformation at the corresponding time of $t = t_2$.

2.5.3. Phase III: $t_2 < t \leq t_3$

Following Shen and Jones (1992) and Schleyer and Hsu (2000), it is assumed that the membrane force $\bar{N}$ is identically distributed throughout the span of the beam whilst the transverse shear force is negligible at the mid-span. The fully plastic stress conditions at the support and mid-span of the beam are, respectively,

$$|\bar{M}_S|(1-\bar{Q}_S^2) + \bar{N}^2 + \bar{Q}_S^2 = 1, \quad \text{if} \quad |\bar{M}_S| > 0 \tag{41a}$$

$$\bar{N}^2 + \bar{Q}_S^2 = 1, \quad \text{if} \quad |\bar{M}_S| = 0 \tag{41b}$$

and

$$\bar{M}_B + \bar{N}^2 = 1. \tag{42}$$

If motion of the beam member ceases when $D < 1$ (Mode I deformation), this is followed by residual elastic vibration of the beam. By contrast, if motion ceases when $D = 1$, then the beam would fail in either modes II or III.

Phase III motion begins with two existing stationary plastic hinges (one each at the support S and mid-span B), following on from Phase II. A travelling plastic hinge A then develops that moves towards the stationary hinge at the mid-span (Fig 6a) before ending up in a final two-hinge collapse configuration (Fig 6b). The admissible transverse displacement field at the start of Phase

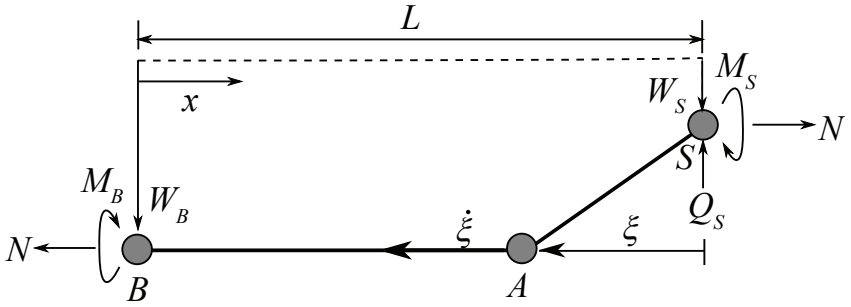

(a) Traveling hinge with $\xi < L$

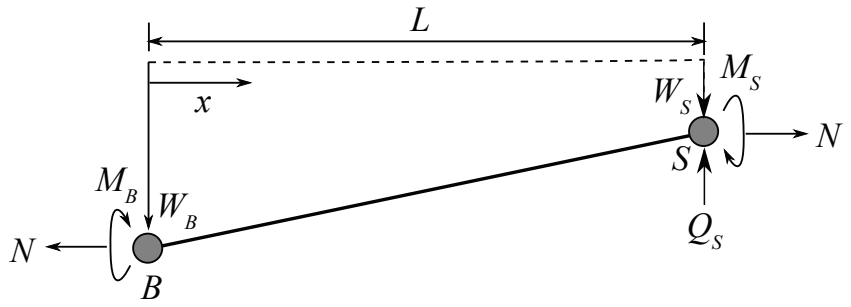

(b) Static hinge with $\xi = L$

Figure 6: Schematic of transverse displacement profile for the right-half of the structural beam system in Phase III (a) before and (b) after the travelling hinge reaches its mid-span.

III motion - see Fig 6a - is (Shen and Jones, 1992)

$$W(x,t) = \begin{cases} w_1(t_1) + w_2(t_2) + w_3(t) & \text{if } 0 \le x \le L - \xi \\ w_4(t) + \Big[w_1(t_1) + w_2(t_2) + w_3(t) - w_4(t)\Big]\frac{L-x}{\xi} & \text{if } L - \xi < x < L \end{cases} \tag{43}$$

where $w_1(t_1)$ and $w_2(t_2)$ are terminating amplitudes of the generalised displacements from Phases I (at time t_1) and II (at time t_2), respectively. When the travelling plastic hinge reaches the mid-span, i.e. $\xi = L$, the admissible transverse displacement field for Fig 6b becomes

$$W(x,t) = w_4(t) + \Big[w_1(t_1) + w_2(t_2) + w_3(t) - w_4(t)\Big]\frac{L-x}{L}. \tag{44}$$

The bending strain energies of the beam member and rotational spring are, respectively,

$$E_B^b(t) = M_B \frac{w_3(t) - w_4(t)}{\xi}, \tag{45}$$

and

$$E_S^b(t) = |M_S| \frac{w_3(t) - w_4(t)}{\xi}. \tag{46}$$

The membrane strain energies of the beam member and the horizontal axial spring may be expressed, respectively, as

$$E_B^m(t) = N\Delta_B(t) \tag{47}$$

and

$$E_S^m(t) = N\Delta_S(t) \tag{48}$$

where $\Delta_B(t) = \Delta(t)/(1 + 1/\sqrt{1 - Q_S^2/Q_0^2})$ is the in-plane membrane displacement at the mid-span, $\Delta(t) = [w_3(t) - w_4(t)]^2/\xi$ is the total membrane displacement and $\Delta_S(t) = \Delta(t) - \Delta_B(t)$ is the membrane displacement at the support. Here, it is assumed that in-plane membrane displacement is significant where a plastic hinge has developed (Schleyer and Hsu, 2000; Langdon and Schleyer, 2005). The shear strain energy of the vertical axial spring is

$$E_S^s(t) = Q_S w_4(t). \tag{49}$$

Note that the parameters M_S, Q_S, N, M_B, ξ and $\dot{\xi}$ in Eqs. 45, 47, 46, 48 and 49 are unknowns. Recasting them in a non-dimensional form, viz. $\bar{M}_S$, $\bar{Q}_S$, $\bar{N}$, $\bar{M}_B$, $\bar{\xi} = \xi/L$ and $\dot{\bar{\xi}} = \dot{\xi}/L$, they will have to be computed as described below.

The non-dimensional velocity of the travelling hinge A is (Shen and Jones,

1992)

$$\dot{\bar{\xi}} = \frac{\sigma_Y}{\rho L^2} \frac{1.5(|\bar{M}_S| + \bar{M}_B) - 2\bar{Q}_S \dot{\bar{\xi}}(L/H)/\sqrt{3} + 6\bar{N}(\dot{\bar{w}}_3 - \dot{\bar{w}}_4) + \bar{\xi}[p(t)/p_c]}{\bar{\xi}(\dot{\bar{w}}_3 - \dot{\bar{w}}_4)} \tag{50}$$

where $\bar{w}_3 = w_3(t)/H$, $\dot{\bar{w}}_3 = \dot{w}_3(t)/H$, $\dot{\bar{w}}_4 = \dot{w}_4(t)/H$; $p_c = 4M_0/L^2$ is the fully plastic collapse force per unit length, i.e. the largest force per unit length that can be supported by the structural beam system when subjected to a pure bending moment before the bending moment at each plastic hinge reaches the fully plastic bending moment M_0 (Jones, 1989). Note that when the travelling hinge A reaches the existing stationary hinge at the mid-span B, they coalesce into a single stationary hinge so that in subsequent motion

$$\dot{\bar{\xi}} = 0 \quad \text{and} \quad \bar{\xi} = 1. \tag{51}$$

The calculations of $\bar{M}_S$, $\bar{Q}_S$, $\bar{N}$, $\bar{M}_B$ would depend on whether damage had initiated. If the state variable $\omega_d < 1$, then $\bar{M}_S$, $\bar{Q}_S$ and $\bar{N}$ are governed by normality requirements so that plastic flow must occur at a non-negative energy dissipation rate since they have met the fully plastic stress condition (Eq. 41). Therefore, according to Shen and Jones (1992),

$$\bar{N}\left(1 + \frac{1}{\sqrt{1 - \bar{Q}_S^2}}\right) = 2(\dot{\bar{w}}_3 - \dot{\bar{w}}_4) \tag{52a}$$

$$\bar{Q}_S\left[\frac{2}{\sqrt{1 - \bar{Q}_S^2}} - \frac{|\bar{M}_S|}{\sqrt{1 - \bar{Q}_S^2}}\right] = \frac{4\bar{\xi}(L/H)\dot{\bar{w}}_4}{\sqrt{3}(\dot{\bar{w}}_3 - \dot{\bar{w}}_4)} \tag{52b}$$

if $|\bar{M}_S| > 0$, and

$$\bar{N}\left[\frac{2\dot{\bar{w}}_4}{\sqrt{3}\bar{Q}_S} + \frac{\dot{\bar{w}}_3 - \dot{\bar{w}}_4}{\bar{\xi}(L/H)}\right] = 2\frac{(\dot{\bar{w}}_3 - \dot{\bar{w}}_4)(\dot{\bar{w}}_3 - \dot{\bar{w}}_4)}{\bar{\xi}(L/H)} \tag{53}$$

if $|\bar{M}_S| = 0$. If the state variable $\omega_d = 1$, then the non-dimensional bending

moment $\bar{M}_S$, membrane force $\bar{N}$ and shear force $\bar{Q}_S$ are governed by Eq. 13. Note that the non-dimensional bending moment $\bar{M}_B$ remains governed by fully plastic stress condition established for the mid-span ($\psi_B^p = 0$) in Eq. 42.

To calculate $\bar{M}_S$, $\bar{Q}_S$, $\bar{N}$ and $\bar{M}_B$, they have to be expressed as functions of $\bar{w}_3$, $\bar{w}_4$, $\dot{\bar{w}}_3$, $\dot{\bar{w}}_4$, $\bar{\xi}$, $\dot{\bar{\xi}}$ and t through Eqs. 41, 42, 50, 52 and 53 if $\omega_d < 1$; and through Eqs. 14, 13, 42 and 50 if $\omega_d = 1$. The temporal evolution of these parameters are obtained by solving the aforementioned equations using the well-known 4th order Runge-Kutta method with the initial conditions of $w_3 = w_4 = 0$ and $\dot{w}_4 = 0$. Following Symonds et al. (1984), the starting amplitude of the generalised velocity $\dot{w}_3$ for Phase III is given by

$$\dot{w}_3 = \frac{12}{\pi^2}\dot{w}_2(t_2) \tag{54}$$

where $\dot{w}_2(t_2)$ refers to the terminating amplitude of the generalised velocity from Phase II at time t_2. Phase III deformation ends at time t_3 if motion of the beam member ceases i.e.

$$\dot{w}_3(t_3) = 0. \tag{55}$$

If the damage variable $D < 1$ when this occurs, then the beam fails in mode I. Otherwise, a mode II or mode III failure would ensue if $D = 1$.

If the structural system fails before all its initial kinetic energy is expended, then the beam member would acquire a residual kinetic energy at the point of severance. Parts of this are absorbed through further plastic deformation as the beam continues to deform until it reaches a rigid permanent set whilst the remaining as translational kinetic energy. In the current model, the energy that is absorbed post failure is not considered. The residual energy and momentum for one-half of the structural beam system at the instant of

failure are given by (Shen and Jones, 1992)

$$E_{ktr} = \frac{1}{2}m(L-\xi)\dot{W}_B^2(t_3) + \frac{1}{2}m\int_{L-\xi}^{L}\left[\dot{W}_S(t_3) + [\dot{W}_B(t_3) - \dot{W}_S(t_3)]\frac{L-x}{\xi}\right]^2 \mathrm{d}x \tag{56}$$

and

$$I_{ktr} = m(L-\xi)\dot{W}_B(t_3) + m\int_{L-\xi}^{L}\left[\dot{W}_S(t_3) + [\dot{W}_B(t_3) - \dot{W}_S(t_3)]\frac{L-x}{\xi}\right]\mathrm{d}x \tag{57}$$

or, in non-dimensional form, as

$$\bar{E}_{ktr} = \frac{E_{ktr}}{E_{\text{ext}}} \tag{58}$$

and

$$\bar{I}_{ktr} = \frac{I_{ktr}}{I_{\text{ext}}} \tag{59}$$

where $I_{\text{ext}} = L\int_0^{t_d} p(t)\,\mathrm{d}t$ is the external momentum, $E_{\text{ext}} = \rho BHLV_0^2/2$ is the external energy and $V_0 = I_{\text{ext}}/\rho HBL$ is the equivalent impulsive velocity.

3. Finite element implementation

3.1. Material properties and damage model

Finite element analyses were performed using ABAQUS (2010). Material description based on the conventional J_2 flow theory is adopted to allow progressive degradation of material stiffness to be implemented in finite elements. This approach, coupled with element deletion, is widely used to model progressive damage and fracture in ductile materials (Hancock and Mackenzie, 1976; Johnson and Cook, 1983). All the beams modelled are made of Aluminium 6061-T6 which is often assumed to be strain rate insensitive (Jones, 1971). Table 1 lists the material properties of the beams tested by Menkes and Opat (1973).

Table 1: Material properties for the Aluminium 6061-T6 beam (Menkes and Opat, 1973)

Density, ρ (kg/m^3)	Young's modulus, E (GPa)	Static yield stress, σ_Y (MPa)	Poisson's ratio
2686	69	283	1/3

The progressive damage model for ductile materials in ABAQUS/Explicit is adopted here. The criterion for ductile damage initiation is given by

$$\omega_d = \int \frac{d\bar{\epsilon}^p}{\bar{\epsilon}^p_d(\eta, \dot{\bar{\epsilon}}^p)} = 1 \tag{60}$$

where ω_d is a state variable that increases monotonically with the equivalent plastic strain. Here, the equivalent plastic strain $\bar{\epsilon}^p_d$ at the onset of ductile damage is assumed to be a function of stress triaxiality η and plastic strain rate $\dot{\bar{\epsilon}}^p$. When Eq. 60 is met, the damage variable D would increase according to (ABAQUS, 2010)

$$\dot{D} = \frac{L_e \dot{\bar{\epsilon}}^p}{\bar{u}^p_f} \tag{61}$$

where $\bar{u}^p_f$ is the effective plastic displacement at failure and $L_e = 7.83\times10^{-4}$ m is the characteristic length of the first-order element used in the FE model. Any element whose stiffness is fully degraded, i.e. $D = 1$, is deleted from the mesh. The two parameters needed to implement a ductile damage model are the damage strain $\bar{\epsilon}^p_d = 0.8$ and the failure displacement $\bar{u}^p_f = 1.1 \times 10^{-2}$ m; both are found through calibration to the experimental data of Menkes and Opat (1973).

In line with the definition of *failure* given in Section 2.4, the FE simulation terminates when a beam member completely detaches from its supports. The smallest impulse needed to induce failure either in mode II or III is referred to here as the critical impulse at mode I→II or II→III transition, respectively (Jones, 1989). To distinguish between failure in mode II and III

in the FE simulations, a separate damage parameter for shear would need to be introduced since a sharp distinction between the two modes is not normally found. The two possibilities are the maximum transverse shear sliding ($\Delta^s_{\max}$) criterion by Jones (1976) and Yu and Chen (2000), or an energy-based criterion by Shen and Jones (1992). However, neither of these are feasible since $\Delta^s_{\max}$ is not a monotonic function of I^* and the plastic work per unit volume (energy density) is a mesh-dependent quantity (Yu and Chen, 2000). Consequently, the critical impulse at mode II→III transition will not be predicted by FE unlike the analytical model in Section 2.

3.2. Mesh, loading and boundary conditions

All the beams modelled have length $2L$, width B and thickness H. Only one-half is modelled since reflective symmetry exists on the plane at $x = 0$, $-B/2 \leq y \leq B/2$ and $-H/2 \leq z \leq H/2$. Figure 7 shows the displacement boundary conditions that were imposed on the plane of symmetry and at the supports. 8-node solid brick elements (C3D8R) with reduced integration and hour-glass control were used. All brick elements have equal dimension of 7.83×10^{-4} m on all sides; hence, a typical beam of $0.203(2L)$ m $\times$ $6.35{\times}10^{-3}(H)$ m $\times$ $25.4{\times}10^{-3}(B)$ m tested by Menkes and Opat (1973) would comprise of 33024 ($129 \times 8 \times 32$) elements in its corresponding FE model. Results of convergence studies - to be presented later in Fig 9 - will show that this is sufficient to capture necking localisation, progressive damage and ductile fracture with acceptable fidelity.

The ductile beam is loaded transversely by a uniformly distributed pressure pulse. Unless otherwise specified, the pressure pulse is assumed to be linearly-decaying, i.e. $p(t) = p_0(1 - t/t_d)$ where p_0 is the peak pressure (given in load per unit length) and t_d is the pulse duration. A pulse duration of $t_d = 0.01$ ms is used here - the same is also used by Shen and Jones (1992). However, it needs to be established that a pulse of finite duration $t_d = 0.01$ can be

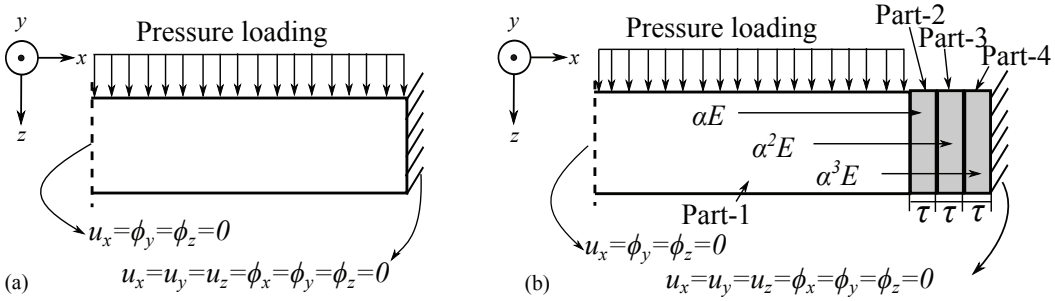

Figure 7: Schematic of boundary, or support, conditions (BCs) in the FE simulations: (a) standard fully clamped BC, and (b) modified BC. u and ϕ denote displacement and rotational degrees of freedom, respectively.

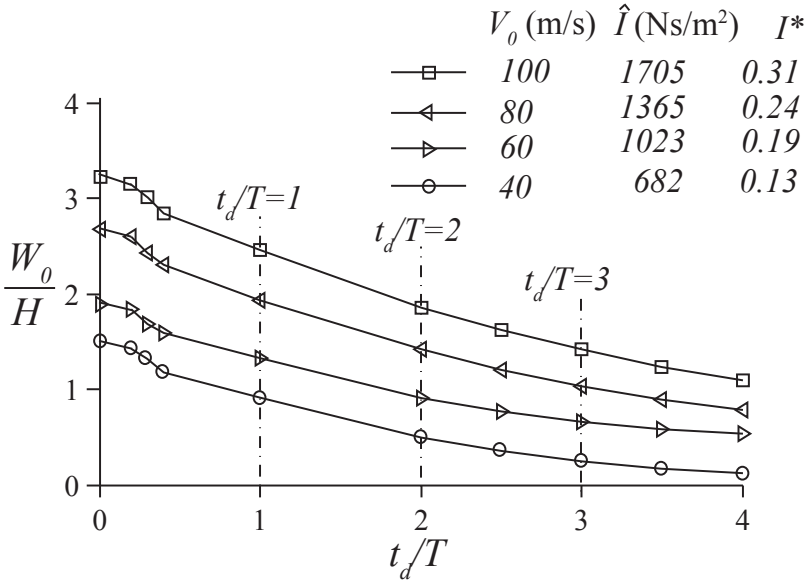

Figure 8: Non-dimensional mid-span displacement W_0/H versus impulse duration t_d/T at different levels of $\hat{I}$. The aluminium beam has dimensions , in metres, of $0.203(2L) \times 6.35\times10^{-3}(H) \times 25.4 \times10^{-3}(B)$.

classed as *impulsive*. Following Xue and Hutchinson (2003), FE simulations were performed to determine the maximum mid-span deflection W_0 for fully-clamped beams subjected to a linearly-decaying pressure loading of different duration t_d. All beams modelled have identical dimensions , in metres, of $0.203(2L) \times 6.35\times10^{-3}(H) \times 25.4\times10^{-3}(B)$ and have material properties

listed in Table 1 - they are identical to the beams tested by Menkes and Opat (1973). The response time T of the beam - defined as the time it takes to attain maximum mid-span deflection under a zero-period impulse ($t_d = 0$ so the beam acquires an instantaneous initial velocity) - was found numerically to be 0.3 ms. Figure 8 shows the variation of the maximum non-dimensional mid-span displacement W_0/H versus pulse duration t_d/T for different levels of impulse per unit area $\hat{I}$, expressed as

$$\hat{I} = \frac{1}{B}\int_0^{t_d} p(t)\mathrm{d}t. \tag{62}$$

For linearly decaying pulse, $\hat{I} = p_0 t_d/2B$. At $t_d/T = 0.4$, the predicted maximum deflection is 12% less than its corresponding zero-period limit. This discrepancy increases to more than 50% at $t_d/T = 3$. This trend is representative of solid beams subjected to pulse-pressure loadings and is independent of pulse shape. Thus, a linearly-decaying pressure pulse of finite duration $t_d = 0.01$ ms is, indeed, impulsive since $t_d/T = 0.033 \ll 0.4$. To simulate non-impulsive loading $t_d/T \gg 3$ should be used. The intensity of loading, for both impulsive and non-impulsive load cases, is characterised by a non-dimensional impulse I^* given by

$$I^* = \frac{\hat{I}}{H\sqrt{\sigma_Y \rho}}. \tag{63}$$

Figure 7a depicts a standard displacement boundary conditions that would need to be imposed for a fully-clamped boundary condition (BC). It is shown later that the local equivalent plastic strain in the beam abutting the supports does not converge with repeated mesh refinement. In order to accurately model progressive ductile fracture at the supports, a modified BC given in Fig 7b is adopted. A similar procedure was previously employed by Yuan and Tan (2013) to model impulsively-loaded rectangular plates. To demonstrate its efficacy, it needs to be demonstrated that both the standard and modified

BCs give similar beam deflection profiles, but only the latter gives a converged equivalent plastic strain at the boundary/support. For the modified BC, three additional parts (labelled 2-4) are added to the end of the original solid beam (part-1) to form an extended boundary shown schematically in Fig 7b. Note that the standard fully-clamped BC of Fig 7a is imposed on part 4. All the additional parts have equal width τ and identical material properties as the solid beam, apart from a gradation of their elastic modulus E, by a factor α. The parameters $\tau = H/6$ and $\alpha = 10$ are obtained by calibration to the experimental data of Menkes and Opat (1973).

Table 2: Number of elements in each direction for Part-1 of the beam with dimensions, in metres, of $0.203(2L) \times 6.35{\times}10^{-3}(H) \times 25.4{\times}10^{-3}(B)$.

Mesh	Number of elements along z-direction	Number of elements along x- direction	Number of elements along y-directions
1	1	16	4
2	2	32	8
3	3	48	12
4	4	64	16
5	5	80	20
6	6	96	24
7	7	112	28
8	8	128	32
9	9	144	36
10	10	160	40

Figure 9 compares the maximum equivalent plastic strain $\overline{\epsilon}^p$ versus mesh density in part-1 for the two BCs. The number of elements in each direction of the beam is listed in Table 2. For a beam with a standard BC (Fig 7a), the maximum $\overline{\epsilon}^p$ must occur next to the supports where tearing is expected to initiate. It is evident that $\overline{\epsilon}^p$ does not converge with repeated mesh refinement for the standard BC. Figure 9 shows that mesh size No.8, with the modified BC, gives sufficiently accurate results and will be used here.

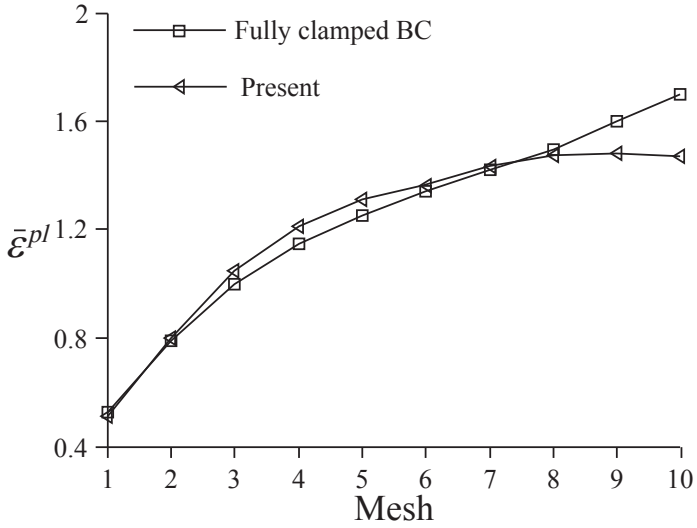

Figure 9: Maximum equivalent plastic strain $\bar{\epsilon}^p$ predicted for part-1 by the FE model. Results shown are for an aluminium beam of dimensions, in metres, $0.203(2L) \times 6.35{\times}10^{-3}(H) \times 25.4{\times}10^{-3}(B)$ subjected to a non-dimensional impulse $I^* = 0.466$ with $t_d = 0.01$ ms. Properties for the aluminium beam is given in Table 1.

Figure 10a compares the deflection profiles predicted by the two BCs which show negligible differences; likewise, for the temporal-history of their mid-span deflection in Fig 10b. Therefore, it is reasonable to conclude that the modified BC also predicts well the mid-span deflection provided necking localisation and ductile fracture had not intervened.

As an additional check, Fig 11 plots the time history of the energies dissipated by a typical beam subjected to a non-dimensional impulsive loading of I^*=0.31 given in Menkes and Opat (1973). Since the pressure impinges only on part 1 of the solid beam, a proportion of the internal and plastic energies are absorbed by the extended boundary (parts 2 to 4). Figure 11 shows that no more than 10% of the total energy is absorbed by the extended boundary during the entire response duration. Even though this would lead to a somewhat smaller final beam deflection in mode I, the excellent comparison between FE predictions and experimental results by Menkes and Opat

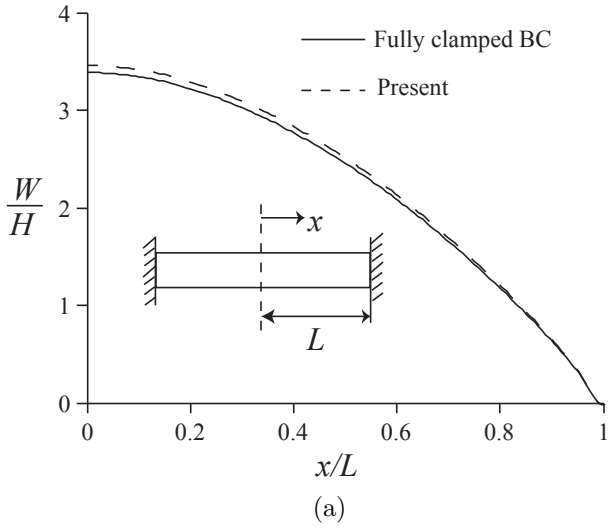

(a)

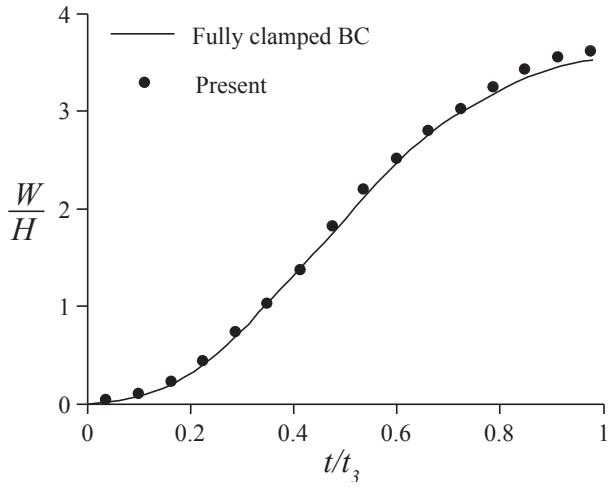

(b)

Figure 10: (a) Deflection profile along the x-axis and (b) temporal-history for the mid-span deflection. Results shown are for aluminium beams of dimensions, in metres, $0.203(2L)$ $\times$ $6.35\times10^{-3}(H)$ $\times$ $25.4\times10^{-3}(B)$ subjected to a non-dimensional impulse of $I^* = 0.354$ with $t_d = 0.01$ ms. Material properties for the beam are listed in Table 1.

(1973) - see Section 4 - suggests that the level of energy loss is acceptable. The causes for non-convergence of the equivalent plastic strain $\overline{\epsilon}^p$, as high-

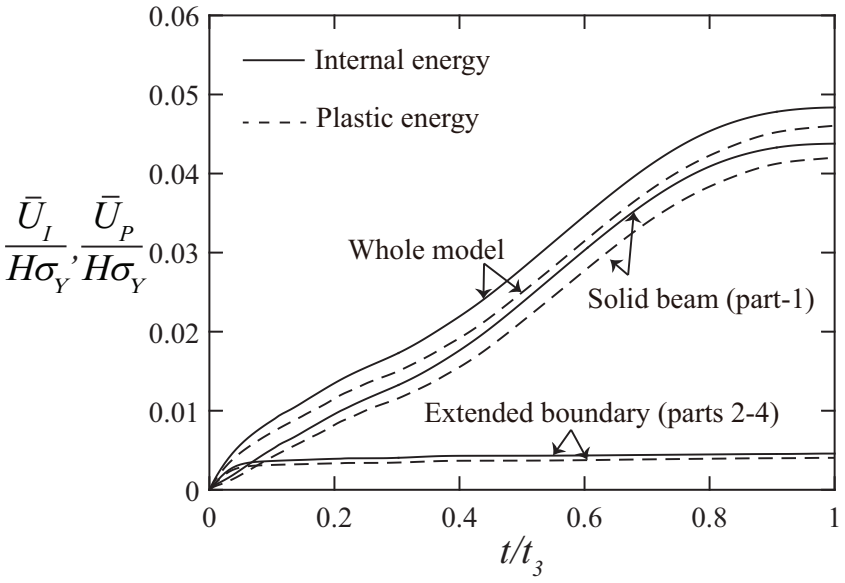

Figure 11: Time history of the non-dimensional internal ($\bar{U}_I/H\sigma_Y$) and plastic ($\bar{U}_P/H\sigma_Y$) energies for a beam of dimensions, in metres, $0.203(2L) \times 6.35{\times}10^{-3}(H) \times 25.4{\times}10^{-3}(B)$ subjected to a non-dimensional impulse $I^*(\triangleq \hat{I}/H\sqrt{\sigma_Y \rho}) = 0.31$.

lighted by Fig 9, is the subject of an on-going investigation, the results from which will be reported elsewhere.

4. Comparison between FE and analytical predictions

All the beam specimens tested by Menkes and Opat (1973) - they have different length ($2L$) and thickness (H) combinations but identical width ($B = 25.4 \times 10^{-3}$ m) - are made of Al 6061-T6 with material properties given in Table 1. The pressure pulse, in both the FE and analytical models, was assumed to be linearly-decaying with a pulse duration $t_d = 0.01$ ms. A flow-chart on the numerical implementation of Section 2 is shown in Fig 12.

Figure 13 compares the predicted mid-span deflection (W_0/H), at either the point of cessation of motion or failure (if complete detachment from

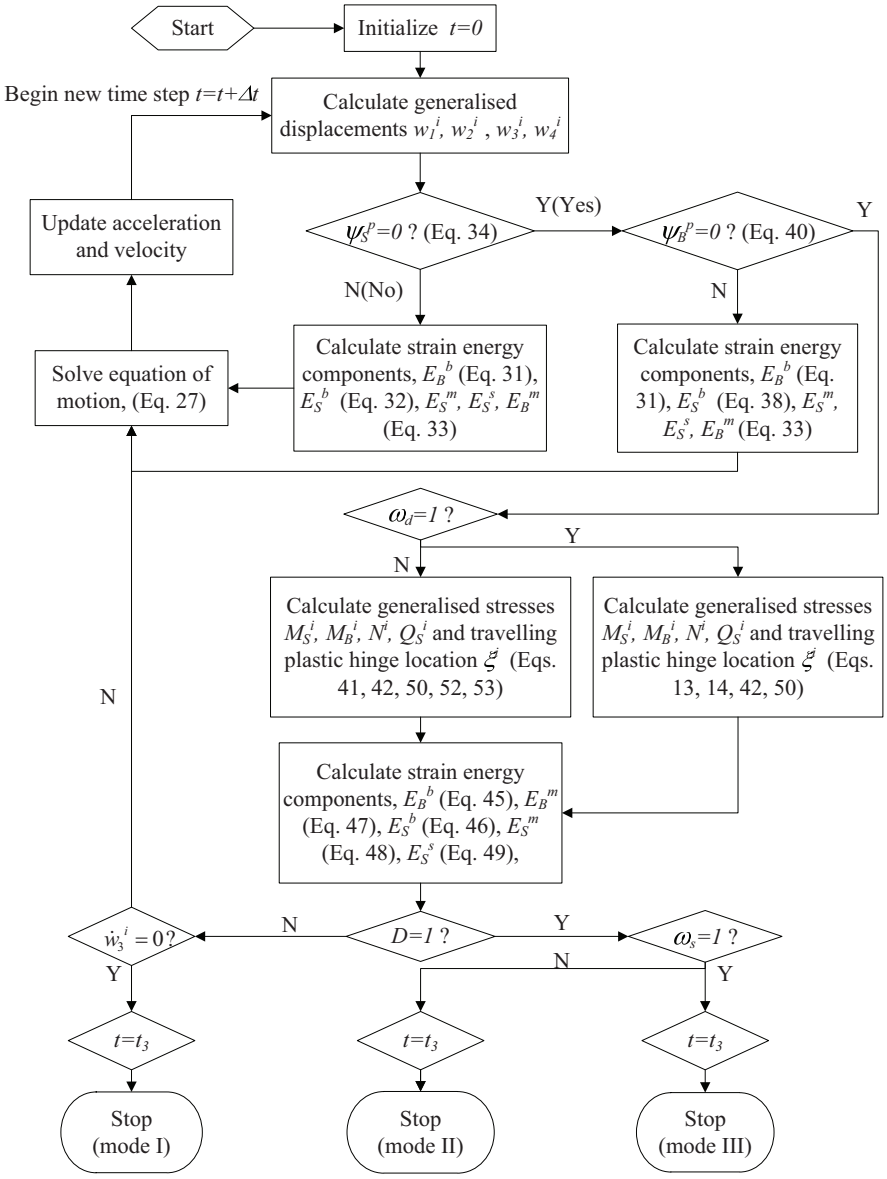

Figure 12: Flow-chart on the numerical implementation of the analytical model in Section 2.

the supports occur), to its corresponding experimental data. The analytical predictions by Shen and Jones (1992) - these are available only for specimens 3 and 5 - are included for comparison. In mode I, there is good agreement

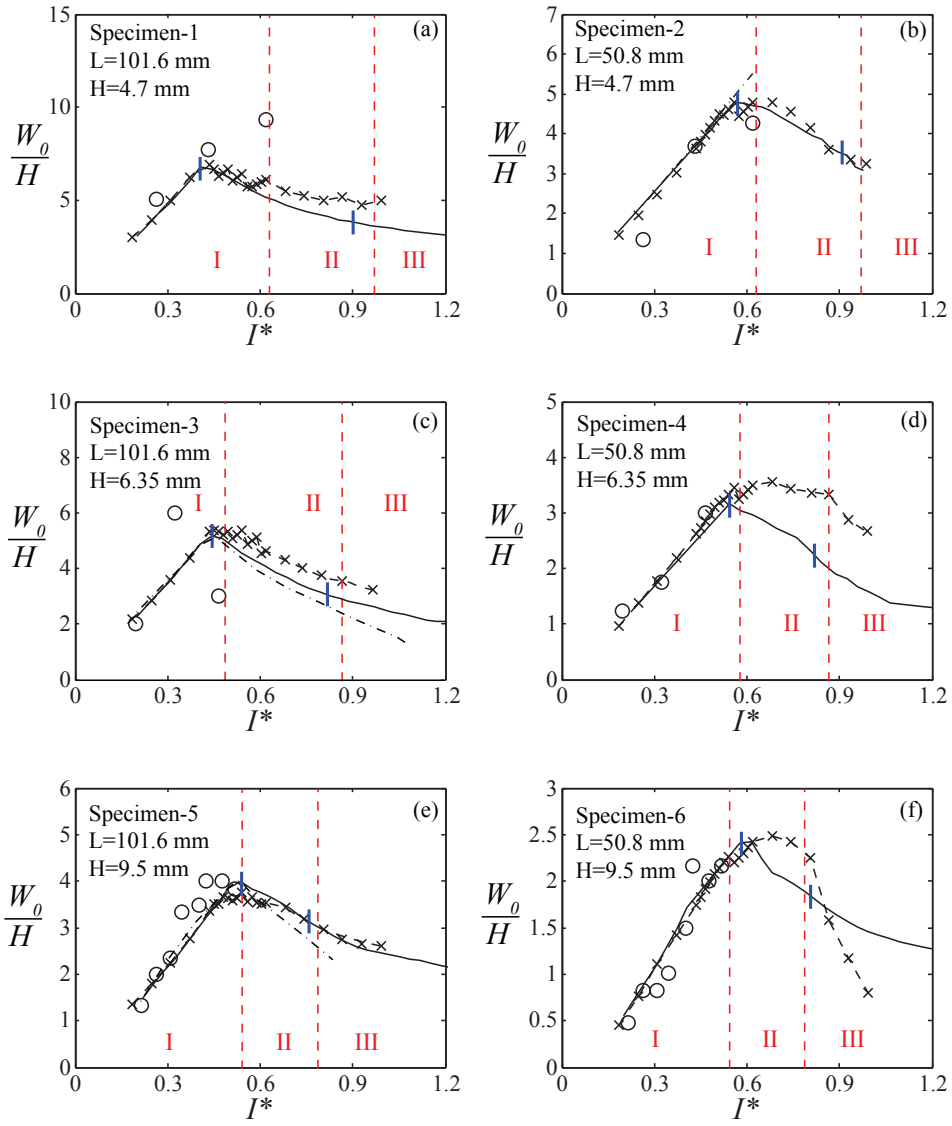

Figure 13: Variations of the non-dimensional mid-span deflection W_0/H with non-dimensional impulse I^*. I, II and III indicates the three distinct damage modes reported by Menkes and Opat (1973). ○ Experimental data by Menkes and Opat (1973); -.-.- Analytical predictions by Shen and Jones (1992); — current analytical model; **|** critical impulse at mode transition by current analytical model; -×- current FE predictions.

between experiments, FE and analytical predictions. The current FE and analytical models correctly predict a reduction in W_0/H with increasing I^*

in modes II and III; they are also broadly in agreement with the predictions by Shen and Jones (1992) for specimens 3 and 5. Apart from specimen 1, the predicted critical impulse at mode I→II and II→III also agree well with those reported by Menkes and Opat (1973).

There is a notable lack of experimental data for modes II and III deformation in Fig 13. To address this, relative mid-span deflections ΔW_0 ($\triangleq W_B(t_3) - W_S(t_3)$) were deduced using existing 'post-test' photographs for specimens 3 and 5 provided by Menkes and Opat (1973). Figure 14 compares this relative mid-span deflection $\Delta W_0/H$ to the current analytical predictions and that by Shen and Jones (1992): a reasonably good agreement for modes I and II is noted. However, the current model over-predicts $\Delta W_0/H$ in mode III since it assumes a constant hinge length of $l = 2H$ - this follows the approach of Wen (1996), Jones (1976) and Alves and Jones (2002a) - instead of re-calibrating for a new hinge length for every data point as employed by Shen and Jones (1992).

Figure 15 shows the 'post-test' deflection profiles in different modes for specimen-3 in Fig 14. Whilst there are discrepancies, the analytical relative mid-span deflection $\Delta W(x = 0) = \Delta W_0$ at mid-span are in excellent agreement with the experiments at each failure modes. The FE predictions of deflection profile $W(x)$ is also included for comparison and, as expected, it is greater than experimental results for $\Delta W(x)$ in modes II and III - the difference is due to the plastic shear sliding distance over the shear band at the support $W_S(t_3)$. Nonetheless, the current FE model successfully captures the different modes of impulsive response observed in a typical beam (specimen-3): large transverse deflection without loss of integrity at the support in mode I, excessive deflection at the mid-span when mode II damage occurs, and no significant deformation in the severed centre region in mode III.

Table 3 compares the critical non-dimensional impulse I^* at mode transi-

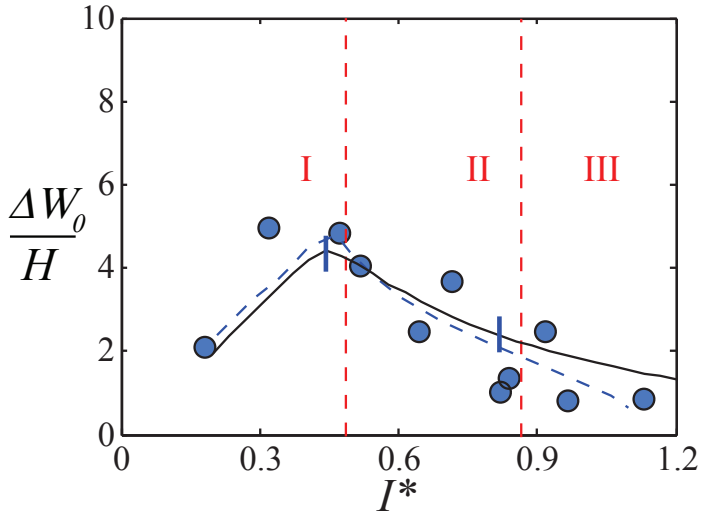

(a) Specimen-3 (0.203 m × 6.35×10^{-3} m × 25.4×10^{-3} m)

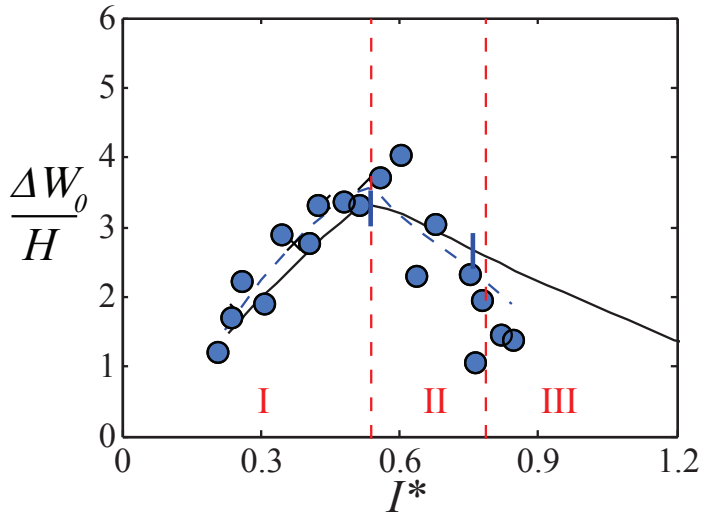

(b) Specimen-5 (0.203 m × 9.47×10^{-3} m × 25.4×10^{-3} m)

Figure 14: Variation of the relative mid-span displacement $\Delta W_0/H$ with non-dimensional impulse I^*. ● experimental data; - - analytical predictions by Shen and Jones (1992); – current analytical predictions; | critical impulse at mode transition by current analytical model.

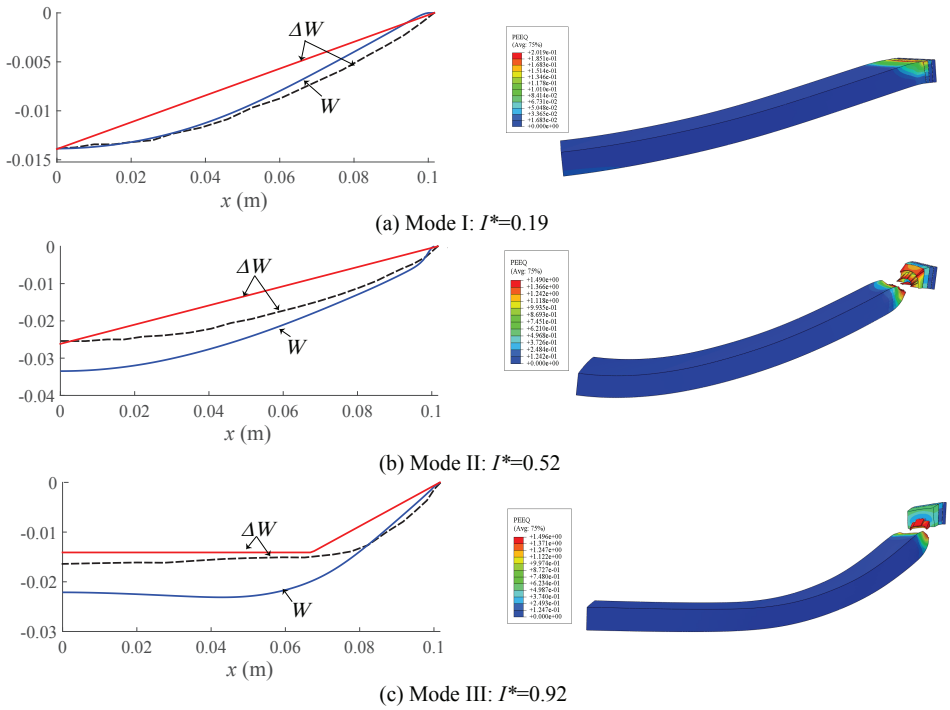

Figure 15: Comparison of the permanent transverse beam deflection profile (Specimen-3 in Fig. 14) for different modes. — : analytical model; — : FE ; - - -: Experiments (Menkes and Opat, 1973).

tions. The current analytical model adopts a rupture strain of $\epsilon_r = 0.5$ (Shen and Jones, 1992) and an effective strain of $\epsilon_d = 0.38$ corresponding to the onset of damage. The latter was obtained by calibrating to the critical I^* corresponding to mode I→II transition for specimen 5. Similarly, for the FE model, $\bar{\epsilon}_d^p = 0.8$ and $\bar{u}_f^p = 1.1 \times 10^{-2}$ m are also obtained through calibration to the aforementioned. Current predictions (FE and analytical) for the critical I^* corresponding to mode I→II transition are in good agreement with the experimental data - as do the predictions by Shen and Jones (1992) - with the notable exception of specimen 1 which is considerably lower. In general, the predicted I^* at mode II→III transition agrees well with experimental data.

Table 3: Critical impulse I^* for mode transitions.

Specimen No	Mode	Current Analytical	Current FE	Analytical[1]	Experiments[2]
1	I $\rightarrow$ II	0.40	0.43	-	0.63
	II $\rightarrow$ III	0.90	-	-	0.97
2	I $\rightarrow$ II	0.57	0.51	-	0.63
	II $\rightarrow$ III	0.92	-	-	0.97
3	I $\rightarrow$ II	0.44	0.43	0.46	0.49
	II $\rightarrow$ III	0.82	-	0.81	0.87
4	I $\rightarrow$ II	0.55	0.54	-	0.58
	II $\rightarrow$ III	0.82	-	-	0.87
5	I $\rightarrow$ II	0.54	0.54	0.54	0.54
	II $\rightarrow$ III	0.76	-	0.76	0.79
6	I $\rightarrow$ II	0.58	0.56	-	0.54
	II $\rightarrow$ III	0.81	-	-	0.79

[1](Shen and Jones, 1992) and [2](Menkes and Opat, 1973).

5. Response to non-impulsive loads

In the previous section, predictions by FE and the current analytical model are validated against experimental data for impulsive loads. Both will now be employed to investigate the dynamic response of elasto-plastic beams to non-impulsive loads. Two of the beams - specimens 3 and 5 - will be modelled here. Unless otherwise specified, a linearly decaying pressure pulse is always prescribed.

5.1. Mid-span deflection and critical impulse at mode transitions

Figure 16 plots the non-dimensional mid-span deflection W_0/H against I^* for pulse durations between $0.01 \leq t_d \leq 2$ ms. Note that $t_d = 0.01$ ms corre-

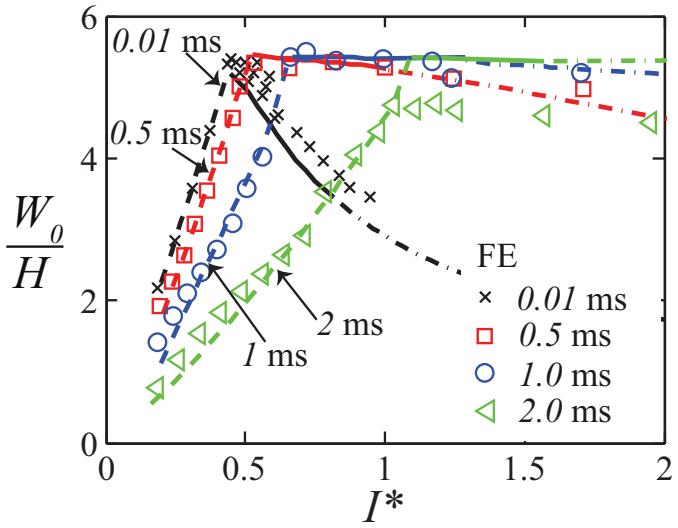

(a) Specimen-3 (0.203 m × 6.35×10^{-3} m × 25.4×10^{-3} m)

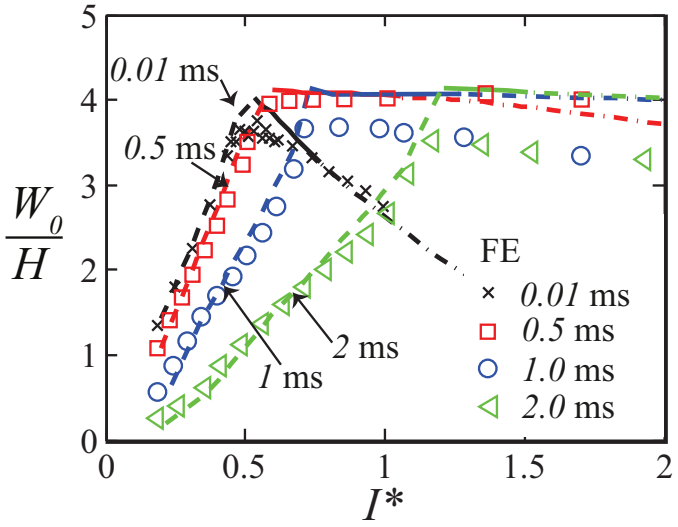

(b) Specimen-5 (0.203 m × 9.47×10^{-3} m × 25.4×10^{-3} m)

Figure 16: Variation of the non-dimensional mid-span deflection W_0/H against non-dimensional impulse I^* for a linearly decaying pressure with different pulse durations. Black lines ($t_d = 0.01$ ms) correspond to impulsive loads. Current analytical predictions: - - - mode I; — mode II; -.-.- mode III.

Table 4: Predicted critical impulse I^* by the analytical (and FE) model for different pulse duration t_d.

Specimen No	Mode	t_d 0.01 ms	t_d 0.5 ms	t_d 1.0 ms	t_d 2.0 ms
3	I $\rightarrow$ II	0.44 (0.43)	0.51 (0.50)	0.66 (0.64)	1.09 (1.03)
	II $\rightarrow$ III	0.82 (-)	0.99 (-)	1.27 (-)	1.56 (-)
5	I $\rightarrow$ II	0.54 (0.54)	0.60 (0.57)	0.74 (0.71)	1.21 (1.18)
	II $\rightarrow$ III	0.76 (-)	1.06 (-)	1.28 (-)	1.51 (-)

sponds to impulsive loading - see Section 3.2. There is excellent agreement between the FE and analytical predictions. Current FE simulations show that beam failure always occurs at the supports regardless of pulse duration t_d which is the reason why failure criteria was established only for the supports in Section 2.4. The results in Fig 16 can be summarised as follows: (1) A broadly similar overall trend for the mid-span deflection with I^* for both impulsive and non-impulsive loads, i.e. W_0/H increases initially before reducing with I^*; (2) At any given I^*, the mode I deflection reduces with increasing t_d whilst the reverse occurs in mode II; (3) The mid-span deflection at mode I$\rightarrow$II transition is insensitive to t_d; and, (4) Mode III deflection for non-impulsive loads are considerably higher than its corresponding impulsive counterpart at the same I^*.

Table 4 compares the predicted critical impulse by the analytical model and FE. The results show that I^* for mode I$\rightarrow$II transition increases with pulse duration t_d. In a similar vein, this is also observed for the corresponding mode II$\rightarrow$III transition. It is worth noting that for impulsive loads, the non-dimensional critical impulse I^* for mode II$\rightarrow$III transition depends only on material properties (Jones, 1976; Yu and Chen, 2000); by contrast, it is shown here that the critical I^* increases with the pulse duration for non-impulsive loadings.

5.2. Partitioning of energy

A non-dimensional strain energy is first introduced - defined as the ratio of the total potential (strain) energy of the structural beam system to the work done by the external pressure loading E^T at the point of cessation of beam motion or at failure - as follows:

$$\bar{E}^P = \frac{E^P (= E_S^b + E_S^m + E_S^s + E_B^b + E_B^m)}{E^T \left(= \int_0^{t_3} p(t) [\int_0^L \dot{W}(x,t) \mathrm{d}x] \mathrm{d}t \right)}. \tag{64}$$

Figure 17 plots the variation of $\bar{E}^P$ versus I^* for different pulse duration t_d where it shows an excellent agreement between the FE and analytical predictions. Notice that $\bar{E}^P$ remains at unity throughout mode I implying that the external work is dissipated entirely through the various plastic work components by the structural beam system. Beyond the mode I→II transition, $\bar{E}^P$ drops dramatically suggesting that a finite amount of residual energy remains in the beam post failure. The effect of pulse duration t_d upon this residual energy (and momentum) will be further discussed in Section 5.3. For a given I^*, increasing the pulse duration t_d has the dramatic effect of increasing the non-dimensional strain energy of a beam failing in modes II or III. This is consistent with the results shown in Fig 16 since more non-dimensional potential (strain) energy is absorbed through larger mid-span deflection.

The components of plastic work absorbed at the *supports* through bending, membrane and shear deformation are non-dimensionalised as follows:

$$\bar{E}_S^b = \frac{E_S^b}{E_S^s + E_S^b + E_S^m}, \quad \bar{E}_S^m = \frac{E_S^m}{E_S^s + E_S^b + E_S^m}, \quad \text{and} \quad \bar{E}_S^s = \beta = \frac{E_S^s}{E_S^s + E_S^b + E_S^m} \tag{65}$$

where $\bar{E}_S^b + \bar{E}_S^m + \bar{E}_S^s = 1$. Figure 18 plots the 3 components of plastic work at the supports against I^* at the point of cessation of beam motion or at failure. The overall trend between the non-dimensional energy components and I^*

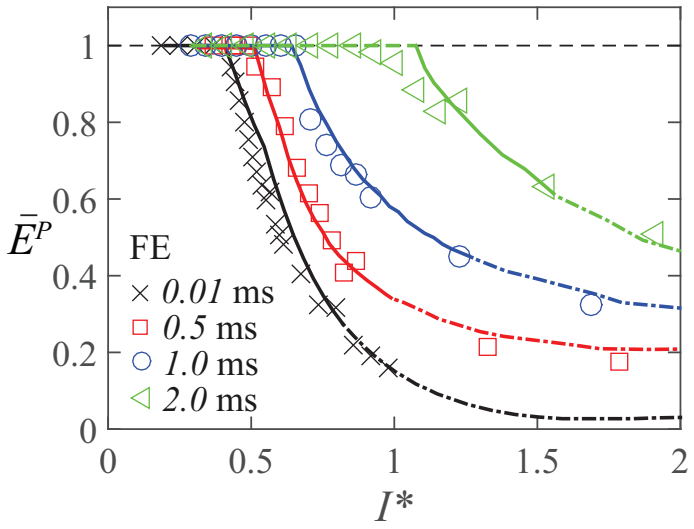

(a) Specimen-3 (0.203 m × 6.35×10^{-3} m × 25.4×10^{-3} m)

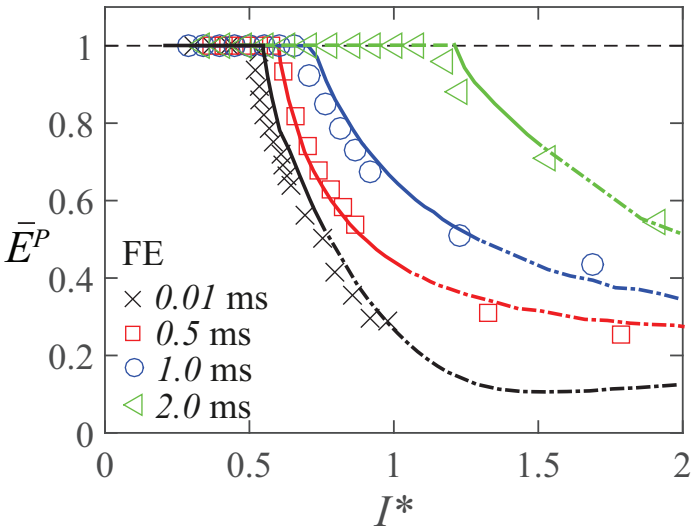

(b) Specimen-5 (0.203 m × 9.47×10^{-3} m × 25.4×10^{-3} m)

Figure 17: Non-dimensional strain energy $\bar{E}^P$ for the two specimens shown in Fig 16. Black lines ($t_d = 0.01$ ms) correspond to impulsive loads. - - - denotes mode I; — denotes mode II; -.-.- denotes mode III.

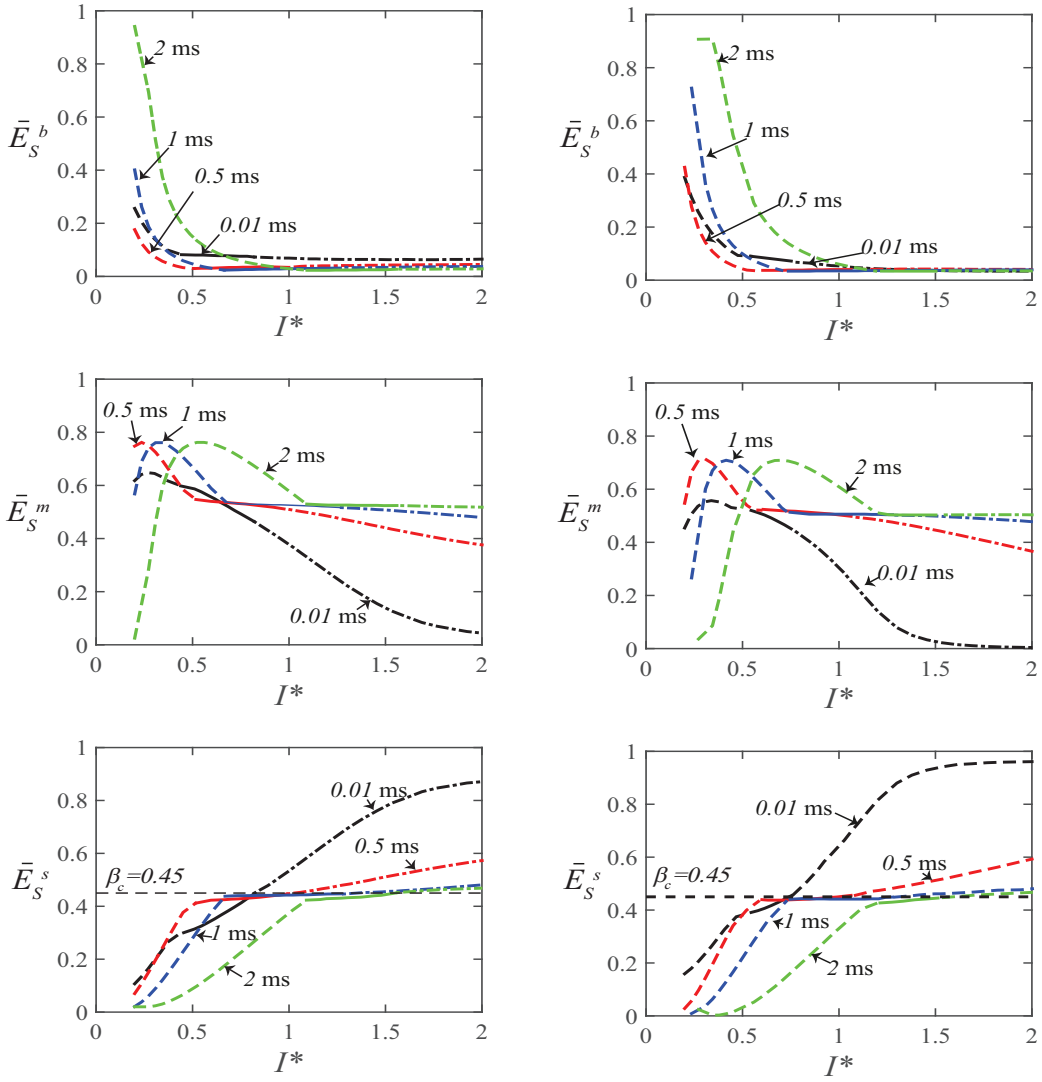

(a) Specimen-3 (0.203 m × 6.35×10^{-3} m × 25.4×10^{-3} m)

(b) Specimen-5 (0.203 m × 9.47×10^{-3} m × 25.4×10^{-3} m)

Figure 18: Components of the plastic work absorbed through bending, membrane and shear deformation at the *supports* for the specimens shown in Fig 16. Black lines ($t_d = 0.01$ ms) correspond to impulsive loads. - - - denotes mode I; — denotes mode II; -.-.- denotes mode III.

are: (1) $\bar{E}_S^b$ reduces monotonically with I^*; (2) $\bar{E}_S^m$ increases initially, reaching a peak value, before reducing with I^*; and, (3) $\bar{E}_S^s$ increases monotonically with I^*. In general, Figure 18 shows that failure at the supports - in modes II and III - for both impulsive and non-impulsive loadings are primarily through a combination of membrane and shear deformations. It is worth noting the critical β value ($\beta_c = 0.45$) marking the transition from mode II→III is obtained based on impulsive load cases - see Shen and Jones (1992) and Yu and Chen (2000). A higher β_c value would require a higher critical I^* to induce mode II→III transition with a corresponding reduction in the mid-span deflection at the mode transition - see Fig 16.

Several studies (Li and Jones, 2000; Shen and Jones, 1992; Yu and Chen, 2000; Jones, 1976) have found that under impulsive loading, the mode II and III deformation is dominated by membrane and transverse shear, respectively. Beyond the mode I→II transition, Figure 18 shows a reduction in the non-dimensional shear strain energy $\bar{E}_S^s$ and an increase in the non-dimensional membrane energy $\bar{E}_S^m$ with t_d for a given I^*. The reduction in $\bar{E}_S^m$ (and increase in $\bar{E}_S^s$) becomes less evident with increasing pulse duration. Notwithstanding, the results above are consistent with the previous studies for impulsively loaded beams (Li and Jones, 2000; Shen and Jones, 1992; Yu and Chen, 2000): i.e., membrane and transverse shear play key roles when inducing mode II damage and the effects of bending is negligible in mode III damage.

5.3. Residual momentum and energy

The 'post-failure' residual momentum $\bar{I}_{ktr}$ and residual energy $\bar{E}_{ktr}$ of the two beams are plotted in Fig 19. Beyond the mode I→II transition, both $\bar{I}_{ktr}$ and $\bar{E}_{ktr}$ increases rapidly with I^*; this is particularly evident for impulsively-loaded beams. Shen and Jones (1992) found that the maximum loss of momentum for impulsively-loaded beams ($t_d = 0.01$ ms) occurs in the vicinity

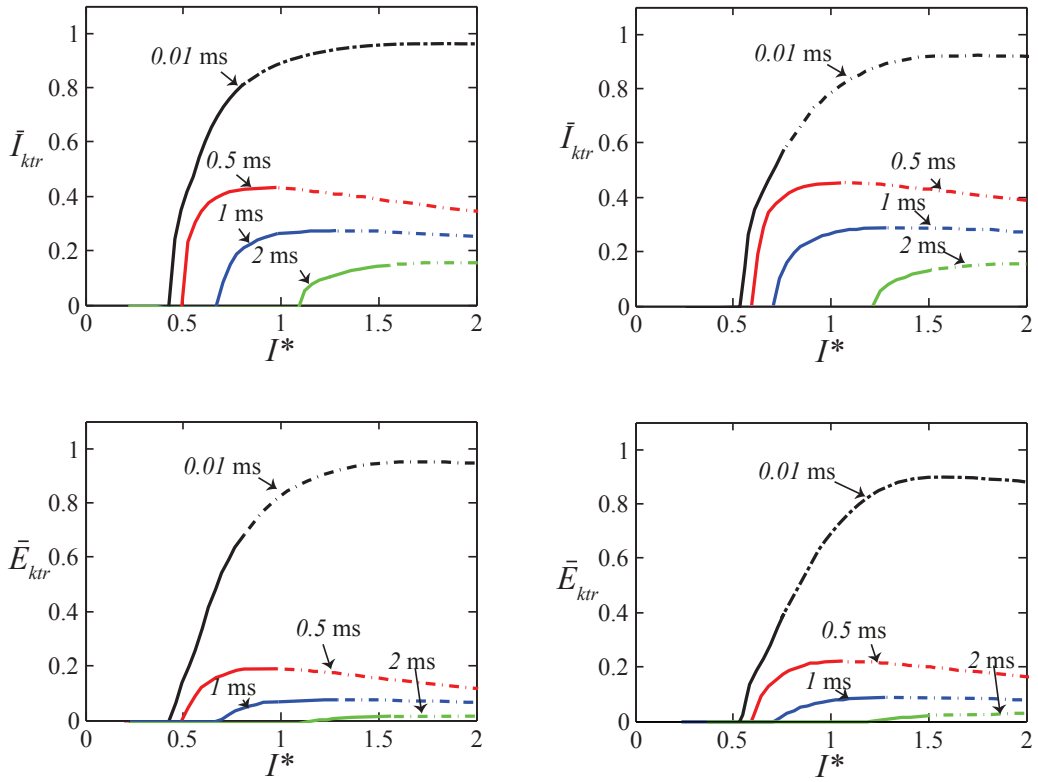

(a) Specimen-3 (0.203 m $\times$ 6.35×10^{-3} m $\times$ 25.4×10^{-3} m)

(b) Specimen-5 (0.203 m $\times$ 9.47×10^{-3} m $\times$ 25.4×10^{-3} m)

Figure 19: Non-dimensional residual momentum $\bar{I}_{ktr}$ and energy $\bar{E}_{ktr}$ for the two specimens shown in Fig 16. Black lines (t_d = 0.01 ms) correspond to impulsive loads. — denotes mode II; -.-.- denotes mode III.

of the mode I→II transition and a rapid decrease in momentum loss by the beam occurs in mode II - this is consistent with the corresponding rise in residual momentum seen in Fig 19. Although a large impulse is generally needed to induce failure in mode III by an impulsive load, a significant amount of residual kinetic energy and linear momentum remains in the beam which was also found in Jones (1976). For a given I^*, increasing the pulse duration t_d has the dramatic effect of reducing the residual momentum and energy of the beam failing in modes II and III. This is consistent with Fig 16

where the mid-span beam deflection W_0/H increases with t_d for a given I^*; hence, additional energy is absorbed through additional plastic work leading to a reduction in the residual momentum and energy.

5.4. Pulse shape

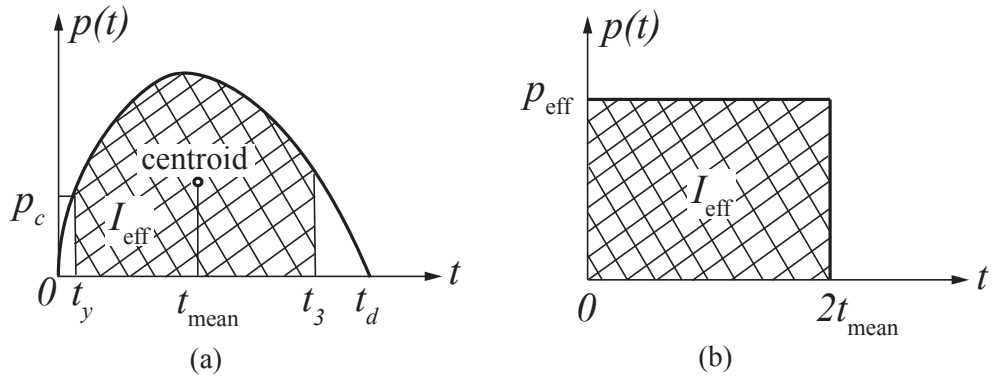

Figure 20: Youngdahl's equivalence parameters for a general pulse: (a) definitions for I_{eff} and t_{mean}; (b) an equivalent rectangular pulse.

All the previous analytical predictions were based on a linearly-decaying pressure pulse given by $p(t) = p_0(1 - t/t_d)$. Here, we will establish whether the approach of Youngdahl (1970, 1971) - see schematic in Fig 20 - may be used to eliminate the effects of pulse shape when investigating the dynamic response of elasto-plastic beams. Following Youngdahl (1970, 1971), an effective impulse (per unit length) is first obtained as follows:

$$I_{\text{eff}} = \int_{t_y}^{t_3} p(t)\mathrm{d}t, \tag{66}$$

where $p(t)$ is the actual pressure pulse, t_3 is time at the end of Phase III motion (see Section 2) and t_y corresponds to the time when the effective pressure (Eq. 67) equals the fully plastic collapse force per unit length of the beam, i.e. $p(t_y) = p_c = 4M_0/L^2$. From Eq. 66, an effective pressure may be

defined as

$$p_{\text{eff}} = \frac{I_{\text{eff}}}{2t_{\text{mean}}} \tag{67}$$

where t_{mean} is the centroid of the effective pressure pulse in Fig 20a given by

$$t_{\text{mean}} = \frac{1}{I_{\text{eff}}} \int_{t_y}^{t_3} p(t)\mathrm{d}t. \tag{68}$$

It is worth noting that Youngdahl (1970, 1971) equivalence parameters were originally defined based on the rigid-perfectly plastic idealisation of dynamically loaded structures.

A parametric study was carried out using different pulse shapes, viz. linearly-decaying (LIN), triangular (TRI), cosine (COS) and sine (SINE), of identical impulse per unit area ($\hat{I} = \int_0^{t_d} p(t)\mathrm{d}t/B$) impinging on a $0.203(2L)$ m $\times$ $6.35\times10^{-3}(H)$ m $\times$ $25.4\times10^{-3}(B)$ m elasto-plastic beam. Figure 21 compares the predicted mid-span deflection at the cessation of beam motion (mode I) or at failure (mode II or III) of the aforementioned pulses to their corresponding Youngdahl's equivalent (Eqs. 67 and 68). The results show that Youngdahl's approach gives an excellent approximation of the mid-span deflection in all three modes for impulsive loadings ($t_d = 0.01$ ms). However, this is not generally the case if the loading is non-impulsive. For monotonically decaying pressure pulses (LIN and COS) that are non-impulsive - see Figs 21a and 21b - a reasonable agreement is observed up until $t_d = 1$ ms beyond which significant discrepancies arise. For non-monotonic pulses (TRI and SINE), the discrepancies between the actual pulse and its Youngdahl's equivalent increases dramatically with t_d. The discrepancies arise because Youngdahl's equivalence parameters were defined based on a rigid, perfectly-plastic idealisation of the loaded structures. Hence, the effective impulse I_{eff} in Eq. 66 does not account for contributions from the elastic response, i.e. it ignores $\int_0^{t_y} p(t)\mathrm{d}t$, which leads to an under-prediction of the mid-span deflection in mode I.

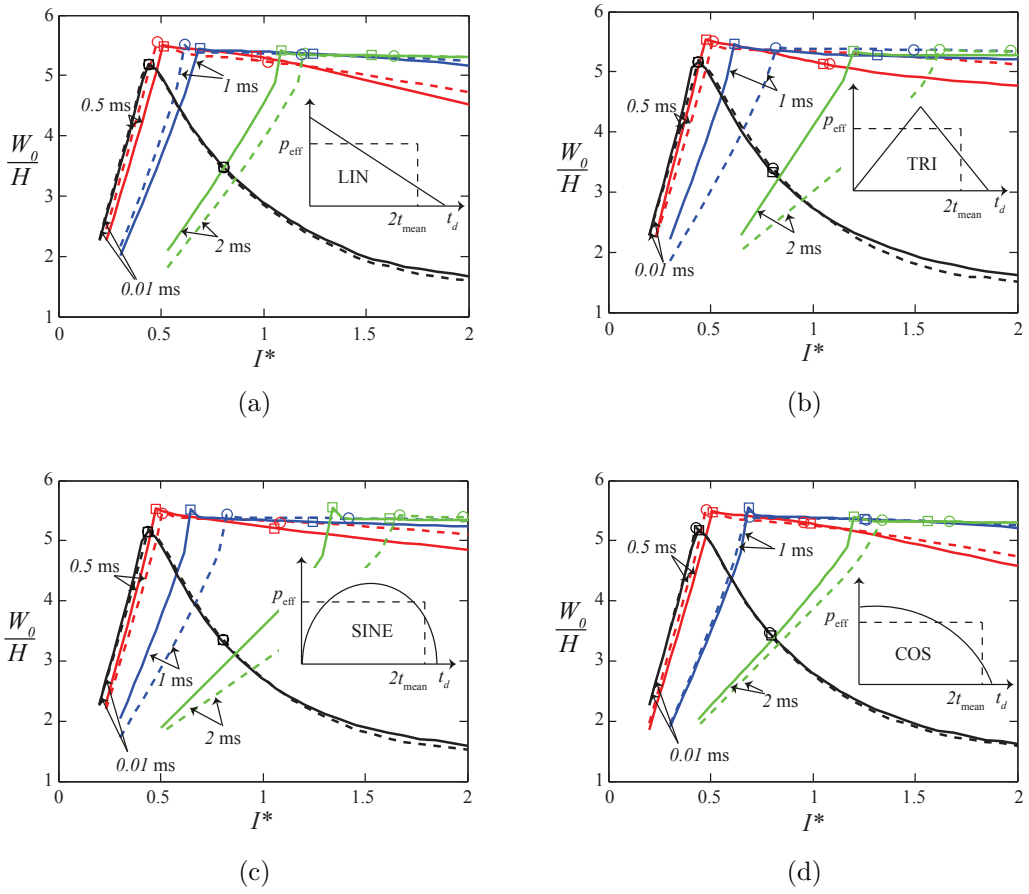

Figure 21: The predicted mid-span deflection at the cessation of beam motion (mode I) or at failure (mode II or III) for four different pressure pulses and their corresponding Youngdahl's equivalent. — analytical prediction by actual pressure pulse; − − − analytical predictions by Youngdahl's equivalent. Black lines ($t_d = 0.01$ ms) correspond to impulsive loads. □ and ○ are critical impulses predicted using the actual pulse and Youngdahl's equivalent.

6. Conclusions

The response of elasto-plastic beams to impulsive and non-impulsive loadings were investigated in this paper. Predictions by the current analytical and FE models were shown to be in good agreement with the experimental results of

Menkes and Opat (1973). Excellent agreement between the predictions were also seen for elasto-plastic beams subjected to non-impulsive loads.

Key findings on the effects of pulse duration on the dynamic response of elasto-plastic beams are as follows: (i) Mode I deflection reduces with increasing pulse duration for a given dimensionless impulse I^* whilst the reverse occurs for the deflection in mode II; (ii) At the transition between mode I and II, the mid-span displacement is insensitive to pulse duration t_d; (iii) Mode III deflection under non-impulsive loads are considerably higher than its corresponding impulsive counterpart at the same I^*; (iv) An increase in the pulse duration t_d delays the transitions (I$\rightarrow$II and II$\rightarrow$III) between deformation modes; (v) Increasing the pulse duration t_d leads to a reduction in the non-dimensional shear energy $\bar{E}_S^s$ but an increase in the non-dimensional membrane energy $\bar{E}_S^m$ at the same I^*; (vi) Increasing the pulse duration t_d decreases the residual momentum and energy of the beam in modes II and III.

It was also shown that Youngdahl's approach can successfully eliminate the dependence of the mid-span deflection of elasto-plastic beams to pulse shape for monotonically decaying, impulsive and non-impulsive, loadings. However, the same would under-predict the mode I mid-span deflection if the loading is non-impulsive and non-monotonically decaying (such as triangular and sine pulses).

Acknowledgment

The authors are grateful to the DE&S Sea Systems Group (Mr. David Manley - Ministry of Defence, UK) and Lloyd's Register Marine (Dr. Fai Cheng - Head of Strategic Research and Technology Policy) for financial support. This work is also funded, in part, by the EPSRC under grant number EP/I028811/1.

References

ABAQUS, 2010. *User's Manual Version 6.10*, Dassault Systemes Simulia Corp., Providence, RI.

Alves, M., Jones, N., 2002a. Impact failure of beams using damage mechanics: Part i - analytical model. Int. J. Impact Eng. 27, 837–861.

Alves, M., Jones, N., 2002b. Impact failure of beams using damage mechanics: Part ii - application. Int. J. Impact Eng. 27, 863–890.

Biggs, J., 1964. Introduction to Structural Dynamics. New York: McGraw-Hill.

Fallah, A. S., Louca, L. A., 2007. Pressure-impulse diagrams for elastic-plastic-hardening and softening single-degree-of-freedom models subjected to blast loading. Int. J. Impact Eng. 34, 823–842.

Fallah, A. S., Nwankwo, E., Louca, L. A., 2013. Pressure-impulse diagrams for blast loaded continuous beams based on dimensional analysis. ASME J. Appl. Mech. 80, 051011.

Hancock, J. W., Mackenzie, A. C., 1976. On the mechanisms of ductile fracture in high-strength steels subjected to multi-axial stress states. J. Mech. Phys. Solids 24, 1471–1469.

Izzuddin, B., 2005. A simplified model for axially restrained beams subject to extreme loading. Int. J. Steel Struct. 5, 421–429.

Johnson, G. R., Cook, W. H., 1983. A constitutive model and data for metals subjected to large strains, high strain rates and high temperatures. In: Proceedings of 7th International Symposium on Ballistics, Netherlands, pp. 541.

Jones, N., 1971. A theoretical study of the dynamic plastic behaviour of beams and plates with finite-deflections. Int. J. Solids Struct. 7, 1007–1029.

Jones, N., 1976. Plastic failure of ductile beams loaded dynamically. ASME J. Appl. Mech. 98, 131–136.

Jones, N., 1989. Structural Impact. Cambridge: Cambridge University Press.

Langdon, G. S., Ozinsky, A., Yuen, S., 2014. The response of partially confined right circular stainless steel cylinders to internal air-blast loading. Int. J. Impact Eng. 73, 1–14.

Langdon, G. S., Schleyer, G. K., 2005. Inelastic deformation and failure of profiled stainless steel blast wall panels. part ii: analytical modelling considerations. Int. J. Impact Eng. 31, 371–399.

Li, Q., Jones, N., 2000. Formation of a shear localization in structural elements under transverse dynamic loads. Int. J. Solids Struct. 37, 6683–6704.

Menkes, S., Opat, H., 1973. Broken beams. Exp. Mech. 13, 480–486.

Ramajeyathilagam, K., Vendhan, C., 2004. Deformation and rupture of thin rectangular plates subjected to underwater shock. Int. J. Impact Eng. 30, 699–719.

Schleyer, G. K., Hsu, S. S., 2000. A modelling scheme for predicting the response of elastic-plastic structures to pulse pressure loading. Int. J. Impact Eng. 24, 759–777.

Shen, W., Jones, N., 1992. A failure criterion for beams under impulsive loading. Int. J. Impact Eng. 12, 101–121.

Spranghers, K., Vasilakos, I., Lecompte, D., Sol, H., Vantomme, J., 2013. Numerical simulation and experimental validation of the dynamic response of aluminum plates under free air explosions. Int. J. Impact Eng. 54, 83–95.

Stronge, W. J., Yu, T. X., 1993. Dynamic Models for Structural Plasticity. Cambridge: Springer-Verlag.

Symonds, P. S., 1985. "A review of elementary approximation techniques for plastic deformation of pulse-loaded structures" In *Metal Forming and Impact Mechanics*. Oxford: Pergamon Press.

Symonds, P. S., Frye, W. G., 1988. On the relation between rigid-plastic and elastic-plastic predictions of response to pulse loading. Int. J. Impact Eng. 7, 139–149.

Symonds, P. S., Kolsky, H., Mosquera, J. M., 1984. Simple elastic-plastic method for pulse loading - comparisons with experiments and finite element solutions. Inst. Phys. Conf. Ser. 70, 479–486.

Wen, H., 1996. Deformation and tearing of clamped work-hardening beams subjected to impulsive loading. Int. J. Impact Eng. 18, 425–433.

Williams, J. H., 1996. Fundamentals of applied dynamic. New York: John Wiley & Sons.

Xue, Z., Hutchinson, J. W., 2003. Preliminary assessment of sandwich plates subject to blast loads. Int. J. Mech. Sci. 45, 687–705.

Youngdahl, C., 1970. Correlation parameters for eliminating the effect of pulse shape on dynamic plastic deformation. ASME J. Appl. Mech. 37, 744–752.

Youngdahl, C., 1971. Influence of pulse shape on the final plastic deformation of a circular plate. Int. J. Solids Struct. 7, 1127–1142.

Yu, T. X., 1993. "Elastic Effects in the Dynamic Plastic Response of Structures" In *Structural Crashworthiness and Failure*. Barking: Elsevier Science Pub.

Yu, T. X., Chen, F. L., 2000. A further study of plastic shear failure of impulsively loaded clamped beams. Int. J. Impact Eng. 24, 613–629.

Yuan, Y., Tan, P. J., 2013. Deformation and failure of rectangular plates subjected to impulsive loadings. Int. J. Impact Eng. 59, 46–59.